

1 **A Comparative Study of Two-way and**
2 **Offline Coupled WRF v3.4 and CMAQ v5.0.2**
3 **over the Contiguous U.S.: Performance**
4 **Evaluation and Impacts of Chemistry-**
5 **Meteorology Feedbacks on Air Quality**

6 Kai Wang¹, Yang Zhang^{1*}, Shaocai Yu^{2*}, David C. Wong³, Jonathan Pleim³, Rohit Mathur³,
7 James T. Kelly⁴, and Michelle Bell⁵

8 ¹Department of Civil and Environmental Engineering, Northeastern University, Boston, MA
9 02115

10 ²Key Laboratory of Environmental Remediation and Ecological Health, Ministry of Education;
11 Research Center for Air Pollution and Health, College of Environment and Resource Sciences,
12 Zhejiang University, Hangzhou, Zhejiang 310058, P.R. China

13 ³Center for Environmental
14 Measurement and Modeling, U.S. EPA, RTP, NC 27711

15 ⁴Office of Air Quality Planning and Standards, U.S. EPA, RTP, NC 27711

16 ⁵School of Forestry & Environmental Studies, Yale University, New Haven, CT 06511

17
18 **Correspondence to:* Yang Zhang (ya.zhang@northeastern.edu); Shaocai Yu (shaocaiyu@zju.edu.cn)

19

20 **Abstract**

21 The two-way coupled Weather Research and Forecasting and Community Multiscale Air
22 Quality (WRF-CMAQ) model has been developed to more realistically represent the atmosphere
23 by accounting for complex chemistry-meteorology feedbacks. In this study, we present a
24 comparative analysis of two-way (with consideration of both aerosol direct and indirect effects)
25 and offline coupled WRF v3.4 and CMAQ v5.0.2 over the contiguous U.S. Long-term (five-year
26 of 2008-2012) simulations using WRF-CMAQ with both offline and two-way coupling modes
27 are carried out with anthropogenic emissions based on multiple years of the U.S. National
28 Emission Inventory and chemical initial and boundary conditions derived from an advanced
29 Earth system model (i.e., a modified version of the Community Earth System Model/Community
30 Atmospheric Model). The comprehensive model evaluations show that both two-way WRF-
31 CMAQ and WRF-only simulations perform well for major meteorological variables such as
32 temperature at 2 m, relative humidity at 2 m, wind speed at 10 m, and precipitation (except for
33 against the National Climatic Data Center data) as well as shortwave/longwave radiation. Both
34 two-way and offline CMAQ also show good performance for ozone (O₃) and fine particulate
35 matter (PM_{2.5}). Due to the consideration of aerosol direct and indirect effects, two-way WRF-
36 CMAQ shows improved performance over offline-coupled WRF and CMAQ in terms of
37 spatiotemporal distributions and statistics, especially for radiation, cloud forcing, O₃, sulfate,
38 nitrate, ammonium, and elemental carbon as well as tropospheric O₃ residual and column
39 nitrogen dioxide (NO₂). For example, the mean biases have been reduced by more than 10 W m⁻²
40 for shortwave radiation and cloud radiative forcing and by more than 2 ppb for max 8-h O₃.
41 However, relatively large biases still exist for cloud predictions, some PM_{2.5} species, and PM₁₀,
42 which warrant follow-up studies to better understand those issues. The impacts of chemistry-

43 meteorological feedbacks are found to play important roles in affecting regional air quality in the
44 U.S. by reducing domain-average concentrations of carbon monoxide (CO), O₃, nitrogen oxide
45 (NO_x), volatile organic compounds (VOCs), and PM_{2.5} by 3.1% (up to 27.8%), 4.2% (up to
46 16.2%), 6.6% (up to 50.9%), 5.8% (up to 46.6%), and 8.6% (up to 49.1%), respectively, mainly
47 due to reduced radiation, temperature, and wind speed. The overall performance of the two-way
48 coupled WRF-CMAQ model achieved in this work is generally good or satisfactory and the
49 improved performance for two-way coupled WRF-CMAQ should be considered along with other
50 factors in developing future model applications to inform policy making.

51 **Keywords:** CMAQ, Two-way coupling, Evaluation, Chemistry-meteorology feedback

52 **1. Introduction**

53 The Community Multiscale Air Quality (CMAQ) modeling system developed by the U.S.
54 Environmental Protection Agency (EPA) (Byun and Schere, 2006; Scheffe et al., 2016; San
55 Joaquin Valley APCD, 2018; Pye et al., 2020; U.S. EPA, 2020) has been extensively used by
56 both scientific community and governmental agencies over various geographical regions and
57 under different meteorological and air pollution conditions to address major key air quality
58 issues such as atmospheric ozone (O₃), acid rain, regional haze, and trans-boundary or long-
59 range transport of air pollutants during the past decades over North America (Zhang et al.,
60 2009a,b; Wang and Zhang, 2012; Hogrefe et al., 2015), Asia (Wang et al., 2009, 2012; Liu et al.,
61 2010; Zheng et al., 2015; Li et al., 2017; Xing et al., 2017; Yu et al., 2018; Mehmood et al.,
62 2020), and Europe (Kukkonen et al., 2012; Mathur et al., 2017; Solazzo et al., 2017). The
63 CMAQ model is traditionally driven offline by the three-dimensional meteorology fields
64 generated separately from other meteorological models such as the Weather Research and
65 Forecasting (WRF) model, and the dynamic feedbacks of chemistry predictions on meteorology

66 are neglected. However, more recently (IPCC, 2018), chemistry-meteorology feedbacks have
67 been found to play important roles in affecting the both global and regional climate change and
68 air quality (Jacobson et al., 1996; Mathur et al., 1998; Ghan et al., 2001; Zhang, 2008; Zhang et
69 al., 2010, 2015a,b, 2017; Grell and Baklanov, 2011; Wong et al., 2012; Baklanov et al., 2014; Yu
70 et al., 2014; Gan et al., 2015a; Wang et al., 2015a; Xing et al., 2015a,b; Yahya et al., 2015a,b;
71 Hong et al., 2017; Jung et al., 2019). Feedbacks of aerosols on radiative transfer through aerosol-
72 radiation interactions (i.e., aerosol direct forcing) and aerosol-cloud interactions (i.e., aerosol
73 indirect forcing) are especially important (Zhang, 2008; Zhang et al., 2015a,b; Baklanov et al.,
74 2014; Wang et al., 2015a; Yahya et al., 2015a,b). Recognizing this importance, as well as the
75 recent advances in knowledge on chemistry-meteorology interactions and computational
76 resources, the U.S. EPA developed a two-way coupled WRF-CMAQ model that accounts for the
77 aerosol direct effect alone (Wong et al., 2012). This version of CMAQ has been applied for both
78 regional and hemispheric studies (Wang et al., 2014; Hogrefe et al., 2015; Xing et al., 2016,
79 2017; Hong et al., 2017, 2020; Sekiguchi et al., 2018; Yoo et al., 2019). For example, Xing et al.
80 (2016) showed that aerosol direct feedbacks may further improve air quality resulting from
81 emission controls in the U.S. and also indicated that coupled models are key tools for quantifying
82 such feedbacks. Reduction in atmospheric ventilation resulting from aerosol induced surface
83 cooling can exacerbate ground level air pollution. Hong et al. (2017) estimated an increase by
84 4.8%-9.5% in concentrations of major air pollutants over China in winter due to incorporation of
85 such effects. Xing et al. (2017) reported that the aerosol direct effects could reduce daily max 1h
86 O₃ by up to 39 μg m⁻³ over China in January through reducing solar radiation and photolysis
87 rates. Hong et al. (2020) found that the benefits of reduced pollutant emissions through
88 weakening aerosol direct effects can largely offset the additional deaths caused by the warming

89 effect of greenhouse gases over China. Some of those studies have also found that the missing
90 aerosol indirect effects in WRF-CMAQ may introduce large model biases on their simulations of
91 radiation and thus air quality (Wang et al., 2014; Sekiguchi et al., 2018; Yoo et al., 2019). There
92 has been a growing awareness that both aerosol effects should be considered together to provide
93 greater fidelity in coupling complex atmospheric processes among chemistry, aerosols, cloud,
94 radiation, and precipitation (Grell and Baklanov, 2011). To address this issue and better represent
95 the one-atmosphere modeling capability of CMAQ, Yu et al. (2014) further extended the two-
96 way coupled WRF-CMAQ model by including aerosol indirect effects and improved WRF-
97 CMAQ's capability for predicting cloud and radiation variables.

98 Different from the traditional online integrated air quality models such as the Gas,
99 Aerosol, Transport, Radiation, General Circulation, and Mesoscale Meteorological (GATOR-
100 GCMM) model (Jacobson, 2001), the WRF model coupled with chemistry (WRF/Chem; Grell et
101 al., 2005) and the WRF model coupled with the Community Atmosphere Model version 5
102 (WRF-CAM5; Ma et al., 2013; Zhang et al., 2015a,b; 2017), in which atmospheric dynamics and
103 chemistry are integrated and simulated altogether without an interface between meteorology and
104 atmospheric chemistry (Zhang et al., 2013), two-way WRF-CMAQ (also referred to as the online
105 access model) is created by combining existing meteorology (i.e., WRF) and atmospheric
106 chemistry (i.e., CMAQ) models with an interactive interface (Yu et al., 2014). As pointed out by
107 Yu et al. (2014), the main advantage of two-way CMAQ is to allow the existing numerical
108 techniques to be used in both WRF and CMAQ to facilitate future independent development of
109 both models while also maintaining CMAQ as a stand-alone model (the offline capability). In the
110 past, a number of studies have compared and evaluated online vs. offline-coupled model
111 performance (Pleim et al, 2008; Matsui et al., 2009; Wilczak et al., 2009; Lin et al., 2010;

112 Herwehe et al., 2011; Yu et al., 2011; Wong et al., 2012; Zhang et al., 2013, 2016a; Choi et al.,
113 2019). However due to the missing offline-coupled mode or component for most online-coupled
114 models, many of those intercomparison studies are subject to some key limitations such as
115 inconsistent model treatments in chemical options (Matsui et al., 2009; Lin et al., 2010; Zhang et
116 al., 2013; Choi et al., 2019) or in both physical and chemical options (Wilczak et al., 2009;
117 Herwehe et al., 2011; Zhang et al., 2016a), different domain projection methods or resolutions
118 (Wilczak et al., 2009; Lin et al., 2010; Zhang et al., 2013), or disunified model inputs (Wilczak et
119 al., 2009; Lin et al., 2010; Zhang et al., 2013). Due to the unique coupling approach, two-way
120 WRF-CMAQ can be used to overcome those limitations and set up ideal intercomparisons
121 between online and offline simulations using consistent model treatments (Pleim et al, 2008; Yu
122 et al., 2011; Wong et al., 2012).

123 In this study, we provide a robust examination of model improvements by considering
124 chemistry-meteorology feedbacks and their impacts on the U.S. air quality using the two-way
125 WRF-CMAQ model (same version as in Yu et al., 2014) with both aerosol direct and indirect
126 effects. Long-term (five-year of 2008-2012) simulations using both two-way and offline coupled
127 WRF and CMAQ models are carried out and compared to the best of our knowledge for the first
128 time over the contiguous U.S. (CONUS) with anthropogenic emissions based on multiple years
129 of the U.S. National Emission Inventory (NEI) and chemical initial and boundary conditions
130 (ICONS/BCONS) downscaled from the advanced Earth system model, i.e., an updated version of
131 the Community Earth System Model/CAM5 (CESM/CAM5; He and Zhang, 2014; Glotfelty et
132 al., 2017). Our objectives include 1) perform a comprehensive model evaluation for major
133 meteorological variables and chemical species from this long-term application of the two-way

134 coupled WRF-CMAQ; and 2) conduct a comparative study of two-way and offline coupled WRF
135 and CMAQ to examine the impacts of chemistry-meteorology interactions on U.S. air quality.

136 Compared to previous studies in the literature, there are a few key features of this work.
137 First, the intercomparisons between two-way (or online) and offline WRF-CMAQ are performed
138 here using consistent model configurations including both physical/chemical options and inputs.
139 Second, unlike a few previous intercomparison studies (Pleim et al, 2008; Yu et al., 2011; Wong
140 et al., 2012) using two-way WRF-CMAQ with only aerosol direct effects for relatively short
141 episodes, the model version in this work includes both aerosol direct and indirect effects and
142 simulations are conducted for multiple years to provide more robust assessments. Third,
143 compared to other studies (e.g., Yahya et al., 2015a,b; Choi et al., 2019) focusing on the impacts
144 of chemistry-meteorology feedbacks on meteorology only or limited chemical species, this study
145 performs comprehensive and extensive evaluation and comparison to demonstrate importance of
146 chemistry-meteorology feedbacks on regional meteorology and air quality.

147 **2. Model description, simulation setup, and evaluation protocols**

148 Two sets of five-year (i.e., 2008-2012) long-term simulations are conducted using the two-
149 way coupled WRF v3.4-CMAQ v5.0.2 model with both aerosol direct and indirect effects and
150 the sequentially offline-coupled WRF v3.4 and CMAQ v5.0.2 model, respectively, over the
151 CONUS with 36-km horizontal grid spacing. The vertical resolution for these simulations
152 consists of 34 layers from the surface (~38 m) to 100 hPa (~15 km). The two-way coupled WRF-
153 CMAQ includes estimations of aerosol optical properties based on prognostic aerosol size
154 distributions and composition. These aerosol optical properties are then used to modulate the
155 shortwave radiation budget estimated using the Rapid and accurate Radiative Transfer Model for

156 General circulation (RRTMG) radiation scheme (Iacono et al., 2008) in WRF. Additionally,
157 aerosol indirect effects, including the first (cloud albedo) and second (cloud lifetime) indirect
158 aerosol forcing and the glaciation (ice and mixed-phase cloud lifetime) indirect aerosol forcing
159 are also modeled. More details on the model development of this version of WRF-CMAQ can be
160 found in Yu et al. (2014). On the other hand, the WRF only model calculates the radiation
161 budgets by using prescribed aerosol optical properties such as aerosol optical depth, single
162 scattering albedo and asymmetry parameters and cloud formation by assuming default droplet
163 number concentration and fixed cloud effective radius, which may not be representative for the
164 large regions with complex air pollution conditions. Both the two-way and offline coupled WRF-
165 CMAQ use the same model configurations as shown in Table S1 in the supplementary material,
166 except that prognostic aerosol impacts on radiation and clouds are fully treated in two-way
167 WRF-CMAQ. The physics options include the RRTMG shortwave and longwave radiation
168 schemes, the Asymmetric Convective Model (ACM2) planetary boundary layer (PBL) scheme
169 (Pleim, 2007), the Pleim-Xiu (PX) land-surface scheme (Xiu and Pleim, 2001), the Morrison
170 two-moment microphysics scheme (Morrison et al., 2009), and version 2 of the Kain–Fritsch
171 (KF2) cumulus scheme (Kain, 2004). The chemical options include the Carbon Bond 2005
172 (CB05) chemical mechanism (Yarwood et al., 2005) with additional chloride chemistry (Sarwar
173 et al., 2008), the sixth generation CMAQ aerosol module (AERO6) (Appel et al., 2013), and
174 CMAQ’s aqueous phase chemistry (AQCHEM). In addition, the time steps of dynamics and
175 radiation for two-way WRF-CMAQ are set as 1 min and 15 mins, respectively, and the call
176 frequency for CMAQ in the two-way coupled model is set to be 5 mins.

177 The meteorological ICONs/BCONs are generated from the National Centers for
178 Environmental Prediction Final Analysis (NCEP-FNL) datasets and the chemical

179 ICONs/BCONs are downscaled from a modified version of CESMv1.2.2/CAM5 (He and Zhang,
180 2014; Glotfelty et al., 2017). The chemical ICONs/BCONs generated from CESM simulations
181 consider the year-to-year variation. The CESM simulations have been comprehensively
182 evaluated against surface, remote sensing including satellite data, and reanalysis data for major
183 meteorological and chemical variables over Europe, Asia, North America, and the globe. The
184 results are also compared with other existing global model results and show generally
185 satisfactory/superior performance. The anthropogenic emissions are based on two versions of
186 NEI. NEI 2008 and NEI 2011 are used to cover the 5-year period, i.e., NEI 2008 for 2008-2010
187 and NEI 2011 for 2011-2012, respectively. Biogenic emissions are calculated online using the
188 Biogenic Emissions Inventory System (BEIS) v3 (Schwede et al., 2005). The sea-salt and dust
189 emissions are also generated online by CMAQ's inline modules (Zender et al., 2003; Zhang et
190 al., 2005). Two-way coupled WRF-CMAQ simulations are reinitialized every 5 days for
191 meteorology fields only. We have conducted sensitivity simulations in the past (Wang et al.,
192 2021) and found that a 5-day reinitialization frequency is more suitable to improve the overall
193 simulation quality while preserving chemistry-meteorology feedbacks. The WRF-only
194 simulations apply the same reinitialization method to make sure any deviation between two
195 simulations are more determined by the feedback processes.

196 The model evaluation in this work mainly focuses on the long-term climatological type of
197 performance in representative seasons (i.e., winter and summer) by comparing 5-year average
198 spatially and temporally matched model predictions of major surface meteorological/radiation-
199 cloud variables and surface/column chemical species against various surface/satellite
200 observations and reanalysis data (The 5-year annual results can be found in the supplemental
201 materials). A brief inter-annual comparison between observations and two-way CMAQ

202 simulations are also performed for selected major meteorological and chemical variables to
203 examine the model's capability in reproducing the year-to-year variations of those variables. The
204 surface meteorological data include temperature at 2 m (T2), relative humidity at 2 m (RH2),
205 wind speed at 10 m (WS10), and wind direction at 10 m (WD10) from the National Climatic
206 Data Center (NCDC), and precipitation from the NCDC, the National Acid Deposition Program
207 (NADP), the Global Precipitation Climatology Project (GPCP), the Parameter-elevation
208 Regressions on Independent Slopes Model (PRISM), and the Tropical Rainfall Measuring
209 Mission Multisatellite Precipitation Analysis (TMPA). The radiation and cloud data include
210 downward shortwave radiation at the ground surface (SWDOWN), net shortwave radiation at the
211 ground surface (GSW), downward longwave radiation at the ground surface (GLW), outgoing
212 longwave radiation at the top of the atmosphere (OLR), and shortwave and longwave cloud
213 forcing (SWCF and LWCF) from the Clouds and the Earth's Radiant Energy System (CERES);
214 aerosol optical depth (AOD), cloud fraction (CF), cloud water path (CWP), and cloud optical
215 thickness (COT) from the MODERate resolution Imaging Spectroradiometer (MODIS); and cloud
216 droplet number concentration (CDNC) derived based on MODIS data by Bennartz (2007). The
217 chemical data include surface O₃ from the Aerometric Information Retrieval System-Air Quality
218 Subsystem (AIRS-AQS) and the Clean Air Status and Trends Network (CASTNET); surface
219 particulate matter with 2.5 μm or less (PM_{2.5}) and its constituents including sulfate (SO₄²⁻),
220 nitrate (NO₃⁻), ammonium (NH₄⁺), elemental carbon (EC), organic carbon (OC), and total carbon
221 (TC = EC + OC) from the Interagency Monitoring of Protected Visual Environments
222 (IMPROVE) and the Chemical Speciation Network (CSN); surface particulate matter with
223 diameters of 10 μm or less (PM₁₀) from the AQS; and column abundance variables such as
224 column carbon monoxide (CO) from the Measurements of Pollution in the Troposphere

225 (MOPITT), tropospheric ozone residual (TOR) from the Ozone Monitoring Instrument (OMI),
226 and column nitrogen dioxide (NO₂) and formaldehyde (HCHO) from the Scanning Imaging
227 Absorption Spectrometer for Atmospheric Chartography (SCIAMACHY).

228 The satellite datasets used in this study are all level-3 gridded monthly-averaged data
229 with various resolutions (i.e., 0.25° for OMI and PRISM, 0.5° for SCIAMACHY, 1° for CERES,
230 GPCP, MODIS, and MOPITT). For the calculation of model performance statistics, the satellite
231 data with different resolutions are mapped to CMAQ's Lambert conformal conic projection
232 using bi-linear interpolation in the NCAR command language. CMAQ model outputs at
233 approximate time of the satellite overpass are paired with the satellite retrievals to facilitate a
234 consistent comparison. Note that only those grid points with valid satellite observations are
235 considered when paring model results with observations, and the averaging kernels are not
236 considered when analyzing the column CO and NO₂ results, which may introduce some
237 uncertainties (Wang et al., 2015b). Modeled CDNC is calculated as the average value of the
238 layer of low-level warm clouds between 950 and 850 hPa as suggested by Bennartz (2007).
239 Following the approach of Wielicki et al. (1996), the SWCF and LWCF are calculated as the
240 difference between the clear-sky and the all-sky reflected radiation at the top of atmosphere for
241 both simulations and observations.

242 The statistical performance evaluation follows a protocol similar to that of Zhang et al.
243 (2006, 2009a) and Yahya et al. (2016) and uses well-accepted statistical measures such as
244 correlation coefficient (R), mean bias (MB), root mean square error (RMSE), normalized mean
245 biases (NMB), and normalized mean error (NME) (S. Yu et al., 2006). Because of different
246 sampling protocols among monitoring networks, the evaluation is conducted separately for
247 individual networks for the same simulated variables/species.

248 3. Comprehensive model evaluation of two-way WRF-CMAQ

249 3.1 Meteorological evaluation

250 3.1.1 Surface meteorological variables

251 Figures 1 shows the spatial distribution of 5-year average MBs for T2, RH2, WS10, and
252 hourly precipitation from two-way WRF-CMAQ against the NCDC data in winter and summer,
253 2008-2012 and Tables 1 and 2 summarize the statistics for the same variables. Most variables
254 except for precipitation show overall moderate to good spatial performance with many sites
255 showing MBs within ± 1.0 °C for T2, ± 10 % for RH2, ± 1 m s⁻¹ for WS10, and ± 0.2 mm hr⁻¹ for
256 precipitation, respectively in both seasons. WRF-CMAQ tends to overpredict T2 (i.e., warm
257 bias) over widespread areas of domain especially along the Atlantic coast, the
258 eastern/southeastern U.S., the Central U.S., and Pacific coast in winter and underpredict T2 (i.e.,
259 cold bias) over the eastern U.S., the Central U.S., and mountainous U.S. in summer, which leads
260 to an overall small warm bias in the whole year (see Figure S1). Similar warm biases of T2 in
261 winter have been previously reported by Cohen et al. (2015) and are found to be associated with
262 the relatively deeper PBL depth using the non-local ACM2 PBL scheme. The relatively larger
263 warm/cold biases over coastal and mountainous areas are likely due to the coarse grid spacing of
264 36-km that cannot well resolve the complex topography (Yahya et al., 2016). Compared to many
265 previous WRF studies (Wang et al., 2012; Brunner et al., 2015; Yahya et al., 2016), which
266 typically show cold T2 biases, the overall small warm biases in this study can be attributed to the
267 soil moisture nudging technique used in the PX land surface scheme (Pleim and Gilliam, 2009).
268 The spatial patterns of MBs for RH2 show a general anti-correlation compared to T2 (i.e., RH2
269 is overpredicted where T2 is underpredicted and vice versa) due to the way how RH2 is

270 calculated based on T2. The spatial distribution of MBs for WS10 also shows dominant
271 overpredictions in both winter and summer especially along coastlines, indicating the prescribed
272 sea-surface temperature might not be sufficient to resolve the air-sea interactions. Systematic
273 overpredictions of hourly precipitation against NCDC data in both seasons are found to be
274 mainly caused by low non-convective precipitation events and can be attributed to the Morrison
275 microphysics scheme (Yahya et al., 2016).

276 The precipitation performance is further examined by comparing WRF-CMAQ with
277 TMPA and PRISM as shown in Figures 2. The spatial distribution of precipitation is well
278 simulated by WRF-CMAQ especially over the CONUS against observations by capturing the hot
279 spots along the Pacific Northwest coast in winter and some areas over the Central U.S. and FL in
280 summer. Moderate overpredictions of precipitation against TMPA over the Atlantic Ocean and
281 Gulf of Mexico in summer are also evident, possibly caused by overprediction of convective
282 precipitation by the Kain-Fritsch scheme (Hong et al., 2017) over ocean. As shown in Tables 1
283 and 2, the domain-average seasonal statistics demonstrate good performance for all variables
284 except for precipitation against NCDC in terms of MBs, NMBs, RMSE, and Rs. For example,
285 the MBs for T2, RH2, WS10, and precipitation are 1.1 °C, 2.2%, 0.57 m s⁻¹, and 0.05-0.23 mm
286 day⁻¹ (except for 0.71 mm day⁻¹ for NCDC) in winter and -1.1 °C, 3.7%, 0.38 m s⁻¹, and 0.13-
287 0.23 mm day⁻¹ (except for 0.75 mm day⁻¹ for NCDC) in summer, respectively, and Rs for those
288 variables are typically between 0.5-0.97, which are well within the performance benchmark
289 values recommended by Zhang et al. (2013) and Emery et al. (2017).

290 Figure 3 shows the bar charts of annual trends for T2, RH2, WS10, and precipitation in
291 2008-2012. Two-way WRF-CMAQ predicts the annual average T2 very well with MBs <
292 0.25 °C in all years. The simulation can also capture the increasing trend of T2 from 2008 to

293 2012 observed by NCDC. RH2 is consistently overpredicted by the two-way WRF-CMAQ in all
294 years despite relatively low biases (MBs < 3%). Both observations and simulations show the
295 lowest RH2 in 2012 and the highest in 2009. As also shown in Figure 1, the model tends to
296 systematically overpredict both WS10 and precipitation throughout all years as well. There are
297 no clear trends (i.e., increasing or decreasing) for WS10 and precipitation between 2008 to 2012
298 from either observations or simulations. However two-way WRF-CMAQ is able to capture both
299 the lowest wind speed and precipitation in 2012 and the highest wind speed in 2008 from
300 observations. In general, the model performs very well in reproducing the year-to-year variation
301 for the major meteorological variables between 2008 to 2012.

302 **3.1.2 Radiation and cloud variables**

303 Figures 4 and 5 compare the 5-year average spatial distribution of major radiation
304 variables (i.e., SWDOWN, GSW, GLW, OLR, and AOD) based on the satellite retrievals and
305 two-way WRF-CMAQ simulations in winter and summer, 2008-2012 and Tables 1 and 2
306 summarize the domain-average model performance statistics. WRF-CMAQ predicts the
307 longwave radiation variables GLW and OLR very well with domain-average of NMBs of -0.3%
308 and 1.8% in winter and -3.6% and 0.9% in summer, respectively, and Rs of 0.96 to 0.99 for both.
309 The shortwave radiation variables SWDOWN and GSW are slightly overpredicted on average
310 with NMBs of 11.3% and 7.5% in winter and 17.1% and 15.1% in summer, respectively, and Rs
311 ranging from 0.75 to 0.99 for both. The simulations also reliably reproduce the spatial
312 distribution of both longwave and shortwave radiation compared to observations in both seasons.
313 The relatively large overpredictions for shortwave radiation especially in summer are very likely
314 caused by the large underpredictions of aerosol direct radiative forcing reflected from the
315 underpredictions of AOD (Figure 5) as well as underprediction of indirect cloud radiative forcing

316 (see Figure 8). It has been reported that WRF v3.4 does not treat the subgrid cloud feedback to
317 radiation, which could also contribute to the overpredictions in shortwave radiation especially in
318 summer (Alapaty et al., 2012; Hong et al., 2017). The model largely underpredicts the magnitude
319 of AOD in both seasons (NMBs of -59.8% in winter and -67.8% in summer), while providing a
320 reasonable representation of the spatial distribution of AOD over the U.S., with generally higher
321 values over the Midwest in winter and over the eastern U.S. in summer. The model also
322 underpredicts the elevated AODs over oceans and the northern part of domain in both seasons.
323 Similar AOD underpredictions have been reported in previous studies over the U.S. using two-
324 way coupled WRF-CMAQ (Gan et al., 2015a; Hogrefe et al., 2015; Xing et al., 2015a). The
325 relatively large underpredictions of AOD may be caused by several factors. First,
326 underprediction of PM_{2.5} concentrations, particularly SO₄²⁻ in both seasons and OC in summer
327 (Tables 3 and 4), can contribute significantly to the underprediction of AOD, especially over the
328 eastern U.S. Second, the underestimation of dust emissions may contribute to missing hot spots
329 from the model over arid areas in CA and AZ (Zender et al., 2003) and underestimates of sea-salt
330 emissions may lead to missing elevated AODs over oceans (Gan et al., 2015b). Third, challenges
331 in adequately representing prescribed and wildfire emissions in the NEI (Kelly et al., 2019) may
332 cause many missing hot spots over large areas of the Pacific Northwest, CA, Canada, and the
333 eastern U.S. especially in summer. Fourth, uncertainties in BCONs of PM_{2.5} concentrations may
334 further contribute to underpredictions of AOD over oceans and the northern part of the domain.
335 For example, Kaufman et al. (2001) found that the background AOD could reach 0.1 over the
336 Pacific Northwest using Aerosol Robotic Network (AERONET) data. The AODs in the current
337 simulation seem to be biased low (between 0.02-0.06 in both seasons over the Pacific Ocean)
338 and indicate potential underpredictions of PM_{2.5} BCONs, especially in the free troposphere.

339 Finally, there are uncertainties associated with MODIS retrievals. Remer et al. (2005) found that
340 the uncertainty of level 3 MODIS monthly AODs can be up to $\pm 0.05 \pm 0.15$ AOD over the land
341 due to clouds and surface reflectance. More AOD data from other satellites or AERONET might
342 be considered in the future work to provide more robust ensemble type of evaluation for AOD.

343 Figures 6-8 compare the 5-year average spatial distribution of major cloud and cloud
344 radiative variables for the satellite retrievals and two-way WRF-CMAQ simulations in winter
345 and summer, 2008-2012 and Tables 1 and 2 summarize the corresponding statistics. As shown in
346 Figures 6 and 7, WRF-CMAQ tends to largely underpredict CDNC, COT, and CWP in both
347 seasons over most of the domain with the domain-average NMBs of -82.4%, -80.8%, and -45.3%
348 in winter and -79.2%, -83.6%, and -66.3% in summer, respectively. Despite the large
349 underprediction of those cloud variables, the spatial correlations are generally predicted well,
350 especially for COT and CWP with Rs ranging from 0.63 to 0.74. Compared to the other cloud
351 variables, CF is much better predicted with an NMB of -10.4% and an R of 0.87 in winter and an
352 NMB of -23.0% and an R of 0.81 in summer, respectively, which is consistent with the
353 performance reported in Yu et al. (2014). The model can reproduce the high CFs over northern
354 and northeastern part of domain as well as over oceans while capturing the low CFs over the
355 mountainous and plateau regions in the U.S. and Mexico especially in winter. In addition to the
356 underprediction of PM_{2.5} (thus underestimating CCN), the large underpredictions of cloud
357 variables (especially CDNC and COT) can be attributed to uncertainties in aerosol microphysics
358 schemes (Yahya et al., 2016) as well as missing aerosol indirect effects on subgrid convective
359 clouds (Yu et al., 2014). Gantt et al. (2014) and Zhang et al. (2015b) also showed the aerosol
360 activation scheme (i.e., Abdul-Razzak and Ghan, 2000) used in the current version of WRF-
361 CMAQ may have underestimated CDNC and thus CWP and COT due to some missing processes

362 such as insoluble aerosol adsorption and giant cloud condensation nuclei. Overall, the relatively
363 poor model performance for cloud variables reflects current limitations in representing aerosol
364 indirect effects and aerosol-cloud interactions in state-of-science online coupled models. Further
365 model improvements that incorporate new knowledge from emerging studies should be
366 conducted in the future.

367 As shown in Figure 8, WRF-CMAQ predictions of SWCF and LWCF generally agree
368 well with the satellite observations in both seasons. The model can capture the elevated SWCF
369 and LWCF over the Atlantic Ocean and widespread areas over the eastern U.S. in winter and
370 those over the Pacific Northwest, northern part of the domain, and Atlantic Ocean in summer.
371 The domain-average NMBs are -11.1% for SWCF and -15.1% for LWCF in winter and -41.3%
372 for SWCF and -33.3% for LWCF in summer, respectively. The relatively larger biases in
373 summer compared to winter are correlated with larger biases associated with radiation and cloud
374 predictions potentially caused by larger underpredictions of aerosol predictions. As discussed
375 earlier, the underpredictions of SWCF may partially contribute the overprediction of SWDOWN
376 (more shortwave radiation reaching the ground) and those of LWCF may further lead to the
377 overpredictions in OLR (more longwave radiation emitted into the space). The performance of
378 SWCF and LWCF is consistent with the 12-km simulation reported in Yu et al. (2014) and even
379 slightly better in terms of NMBs, which might be associated with the long-term vs. short-term
380 simulations. It is also worth noting that SWCF (LWCF) is calculated as the difference between
381 the clear-sky and all-sky shortwave (longwave) radiation at the top of atmosphere, and so
382 performance for SWCF and LWCF depends on performance for both radiation and cloud
383 properties. The generally better performance in terms of model bias for SWCF and LWCF

384 compared to the cloud variables seems to be driven by the relatively good performance of
385 shortwave/longwave radiation in the model.

386 **3.2 Chemical evaluation**

387 **3.2.1 O₃**

388 Figure 9a shows the spatial distribution of simulated average daily maximum 8-h O₃ in
389 summer, 2008-2012 from two-way WRF-CMAQ overlaid with observations from both the
390 AIRS-AQS and CASTNET networks. WRF-CMAQ shows good performance by capturing the
391 spatial distribution of max 8-h O₃ over widespread areas of the domain. The model tends to
392 overpredict O₃ along coastlines in the southeastern U.S., Gulf of Mexico, and Pacific coast,
393 which can be attributed to a poor representation of coastal boundary layers (Yu et al., 2007) and
394 lack of O₃ sink via halogen chemistry (Sarwar et al., 2015) and deposition to water (Gantt et al.,
395 2017). The simulation also underpredicts O₃ in widespread areas in the Midwest, Central, and
396 mountainous regions of the U.S., which is consistent with the results of 36-km simulations from
397 Wang and Zhang (2012) that used an earlier version of CMAQ v4.6 with the same CB05 gas-
398 phase mechanism. In addition to cold T2 biases over those areas (Figure 1), the underpredictions
399 are also believed to be associated with inaccurate representations of precursor emissions and
400 elevated/complex terrain due to the coarse grid spacing of 36-km over those regions. Wang and
401 Zhang (2012) found that their 12-km simulation showed improved performance over similar
402 regions especially in summer.

403 Figure 9c shows the monthly variation of domain-average 5-year average O₃ mixing
404 ratios between observations from AIRS-AQS and simulations from two-way WRF-CMAQ, and
405 Figure 9d shows the diurnal variation of domain-average 5-year average hourly O₃ mixing ratios

406 between observations from CASTNET and simulations from two-way WRF-CMAQ for winter
407 and summer. As shown in Figure 9c, the O₃ mixing ratios are overpredicted throughout the year,
408 which is consistent with overprediction of T2 (figure not shown). The largest overprediction
409 occurs in the relatively cold months such as September to December. It is interesting that the
410 observations show the largest monthly O₃ mixing ratios in spring and early summer while the
411 simulation shows the peak during the summer. The difference in timing of peak O₃ between
412 observations and simulations during the year might be associated with uncertainties in the
413 BCONs of O₃ that reflect impacts of the long-range transport and associated stratosphere-
414 troposphere exchange of O₃. As shown in Figure 9d, WRF-CMAQ tends to overpredict O₃
415 during most hours (i.e., 2:00-18:00) in summer and throughout the whole day in winter partially
416 due to the overprediction of T2, especially in winter (Figure 1). The diurnal pattern of O₃ is
417 captured much better during summer with much less prediction bias, especially during the
418 nighttime, indicating that the model does a better job in predicting the evolution of nocturnal
419 boundary layer and atmospheric chemistry in the warm season than the cold season. The overall
420 overpredictions in this work are also consistent with previous studies (Eder and Yu, 2006; Appel
421 et al., 2007; Wang et al., 2012), although our results show much better nighttime performance
422 owing to the application of the ACM2 scheme that treats both local and non-local closure (Pleim,
423 2007). As also shown in Table 4, the domain-average NMBs and NMEs for max 8-h O₃ in
424 summer are 10.6% and 13.2% against AIRS-AQS and -3.0% and 11.5% against CASTNET,
425 respectively. The statistics are also consistent with previous studies using the CMAQ model
426 (Zhang et al., 2009a; Appel et al., 2013, 2017; Penrod et al., 2014) and can be considered as
427 good performance according to the criteria suggested by Zhang et al. (2013) and Emery et al.
428 (2017).

429 Figure 3 also shows the bar charts of annual trends for max 8-h O₃ from two-way WRF-
430 CMAQ against AQS and CASTNET observations in 2008-2012. Two-way WRF-CMAQ
431 systematically overpredicts O₃ especially against AQS data with MBs typically > 4.0 ppb. The
432 potential reasons for model biases have been discussed earlier in this section. There are no
433 obvious decreasing or increasing trends for max 8-h O₃ from AQS or CASTNET observations.
434 However, the model can generally capture the high O₃ mixing ratios in 2008 and 2010 and the
435 low O₃ mixing ratios in 2009 from both AQS and CASTNET. The similar down and up trends
436 between 2008 to 2010 for O₃ (i.e., decreasing from 2008 to 2009 and increasing from 2009 to
437 2010) from AQS observations were also found by Yahya et al. (2016), but not captured by their
438 simulations. Zhang and Wang (2016) was able to reproduce the similar trend over the
439 southeastern U.S. between 2008 to 2010 using their models and attributed the abnormal high
440 2010 O₃ mixing ratios to the extreme dry and warm weather conditions during fall 2010.

441 3.2.2 Aerosols

442 Figures 10a and 10c shows the spatial distribution of simulated 5-year average PM_{2.5}
443 from two-way WRF-CMAQ overlaid with observations from both the CSN and IMPROVE
444 networks in winter and summer, 2008-2012. As shown, WRF-CMAQ performs well for PM_{2.5}
445 over widespread areas of the Midwest and northeastern U.S. in both seasons, while PM_{2.5} is
446 underpredicted over the southeastern and western U.S. especially in winter. The model also
447 misses some hot spots of observed concentrations in the western U.S., which are mainly caused
448 by TC underpredictions (Figure S6) that are likely linked to poorly allocated and underestimated
449 wildfire emissions in the NEI (Wiedinmyer et al., 2006; Roy et al., 2007; Kelly et al., 2019). The
450 relatively large underpredictions over the eastern U.S. are mainly caused by the combined effects
451 from SO₄²⁻, NH₄⁺, and TC. As shown in Figure S6, WRF-CMAQ largely underpredicts SO₄²⁻ in

452 the Midwest and southeastern U.S. mainly due to the underprediction of oxidants such as O_3 (see
453 Figure 9a) (which leads to less production from the gaseous oxidation), overprediction of
454 precipitation (see Figure 2) (which leads to more wet deposition and removal), and large
455 underprediction of cloud fields (see Figures 6-7) (which leads to less aqueous phase formation),
456 over the same area. On the other hand, NH_4^+ and NO_3^- are either underpredicted or
457 overpredicted, respectively, over the similar areas mainly due to underprediction of SO_4^{2-} .
458 According to the aerosol thermodynamics, when SO_4^{2-} is underpredicted, NH_4^+ tends to be
459 underpredicted due to its major role as cation. More gaseous NH_3 will be available to neutralize
460 NO_3^- , thus leading to overprediction of NO_3^- especially over the sulfate poor regions (West et al.,
461 1999). Other potential reasons include the inaccurate assumptions in the thermodynamic module
462 (for example, the internally mixed aerosol state and equilibrium assumption may not be
463 representative over some regions and different time periods, S. Yu et al., 2006), uncertainties in
464 emissions of key species such as NH_3 and non-volatile cations that affect particle acidity (Mebust
465 et al., 2003; Wang and Zhang, 2014; Vasilakos et al., 2018; Pye et al., 2020), and measurement
466 errors especially for NO_3^- and NH_4^+ (X.-Y. Yu et al., 2006; Karydis et al., 2007; Wang and
467 Zhang, 2012). TC underpredictions over most sites of the domain can be attributed to the
468 underprediction of emissions (e.g., wildfire and primary OC) and underestimation of secondary
469 organic aerosol (SOA) formation (Appel et al., 2017; Pye et al., 2017) since EC (a chemically
470 inert species) is overpredicted, which suggest that atmospheric mixing did not drive the TC
471 underpredictions.

472 Figures 10e and 10f show the monthly variation of 5-year average $PM_{2.5}$ between
473 observations from CSN and IMPROVE, respectively, and simulations from two-way WRF-
474 CMAQ. Both observations and WRF-CMAQ show higher $PM_{2.5}$ concentrations at CSN than

475 IMPROVE for the whole year because most of CSN sites are in more polluted urban areas while
476 majority of IMPROVE sites are in rural areas and national parks. The model tends to
477 underpredict PM_{2.5} over both CSN and IMPROVE sites in the warm months (i.e., April to
478 September) mainly due to the underpredictions of SO₄²⁻ and OC while it overpredicts PM_{2.5} in
479 cold months mainly due to NO₃⁻. The model also captures the seasonality of PM_{2.5} better over
480 CSN sites than IMPROVE sites, especially in the summer months. The large underpredictions
481 over IMPROVE sites during summer months are likely due to the underestimation of precursor
482 emissions (such as wildfire emissions).

483 Figure 11 shows the scatter plots of major PM_{2.5} components such as SO₄²⁻, NH₄⁺, and
484 NO₃⁻, and TC in winter and summer, 2008-2012. The WRF-CMAQ predicts PM_{2.5} constituents
485 well with majority of data within the 1:2 ratio lines in both seasons. Systematic underpredictions
486 of SO₄²⁻ and NH₄⁺ in winter and overpredictions of NO₃⁻ in summer are shown, which are
487 consistent with their spatial distributions. Relatively large under- and overpredictions of TC
488 especially in winter compensate each other and lead to relatively low overall model biases. As
489 also shown in Figure S6, the model fails to reproduce high concentrations of PM₁₀ (those > 20
490 µg m⁻³) over widespread areas of the domain, especially over dust source areas in CA, AZ, and
491 NM. Hong et al. (2017) found the similar large underprediction of dust using CMAQ v5.0.2 over
492 China and attributed it to a too-high threshold for friction velocity in the current dust module
493 (Dong et al., 2016). Sea-salt also seems to be underpredicted by WRF-CMAQ, although sea-salt
494 predictions are better than dust as shown along the coastlines.

495 Figure 3 shows the bar charts of annual averaged observations and simulations for PM_{2.5}
496 over the CSN and IMPROVE sites. Overall, the model performs well for PM_{2.5} for most of years
497 and better over CSN than IMPROVE sites with general underpredictions in most years. The

498 observations for both CSN and IMPROVE show a general decreasing trend, except for 2009
499 over CSN with a strong drop of PM_{2.5} concentrations. According to EPA (2012), the strong drop
500 of PM_{2.5} in 2009 is due to a few reasons including many national and local regulations that are
501 imposed, the contribution of economic slowdown to cleaner air conditions and also favorable
502 meteorological conditions to lower air pollution levels in 2009. The impacts are more apparent
503 over CSN sites mainly composed of urban/suburban areas than IMPROVE sites mainly
504 composed of remote areas and national parks. Two-way WRF-CMAQ is able to reproduce the
505 declining trend well particularly over IMPROVE sites and again demonstrate its capability in
506 accurately simulating the year-to-year variations of not only meteorology but air quality.

507 As recommended by some previous studies (Zhang et al., 2006; Wang and Zhang, 2012;
508 Emery et al., 2017), generally $\pm 15\%$ and $\pm 30\%$ for model biases and 30% and 50% for model
509 errors can be considered as good and acceptable performance. As shown in Tables 3 and 4,
510 WRF-CMAQ in this work demonstrates an overall good or acceptable performance in predicting
511 aerosols in terms of statistics especially for PM_{2.5} in both seasons, NO₃⁻ OC, and TC in winter,
512 and SO₄²⁻ and NH₄⁺ in summer. It shows the domain-average NMBs of -7.2% and 8.6% in winter
513 and -13.2% and -26.9% in summer for PM_{2.5} against CSN and IMPROVE, respectively; NMBs
514 of -10.2% and -20.9% in summer for SO₄²⁻ against CSN and IMPROVE, respectively; NMBs of
515 -0.3% and 13.3% in winter for NO₃⁻ against CSN and IMPROVE, respectively; an NMB of 3.3%
516 for NH₄⁺ in summer against CSN; an NMB of 13.0% in winter for OC against IMPROVE; and
517 NMBs of 7.2% and 17.5% in winter for TC against CSN and IMPROVE, respectively. The
518 relatively large underpredictions of PM₁₀ in both seasons, i.e., NMBs of -36.3% in winter and -
519 45.8% in summer against AQS, indicate further improvements of dust emissions are warranted.
520 Overall, the aerosol performance is also comparable or better than previous CMAQ or WRF-

521 CMAQ applications (Wang and Zhang, 2012; Penrod et al., 2014; Yu et al., 2014). For example,
522 Penrod et al. (2014) showed 5-year (2001-2005) average NMBs of -23.3% and 4.0% in winter
523 and -19.1% to -17.6% in summer for PM_{2.5} against CSN and IMPROVE data over the CONUS
524 using the CMAQ v5.0 and Yu et al. (2014) reported the monthly mean NMBs of -6.2% and -
525 16.8% for PM_{2.5} against CSN and IMPROVE over the eastern U.S. using the same version of
526 WRF-CMAQ as that used in this study.

527 **3.2.3 Column abundance**

528 Figures 12 and 13 show the spatial distribution of 5-year average column abundances
529 between various satellite products and two-way WRF-CMAQ for column CO, TOR, column
530 NO₂, and column HCHO in winter and summer, 2012 and Tables 3 and 4 summarize the
531 statistics. As shown, WRF-CMAQ can reproduce the spatial distribution of the column
532 abundances of gases quite well in both seasons except for column HCHO in winter with Rs
533 ranging from 0.70 to 0.87. TOR in both seasons, column NO₂ in winter and column HCHO in
534 summer are also generally well predicted in terms of magnitudes with NMBs of 4.7% for TOR
535 and 0.3 for NO₂%, respectively, in winter and -8.0% for TOR and 15.0% for HCHO,
536 respectively, in summer. Systematic underpredictions for column CO occur in both seasons over
537 the whole domain with NMBs of -20.5% in winter and -27.8% in summer for a few reasons.
538 First, the BCONs of CO may be significantly underestimated from the CESM model. Using
539 WRF/Chem or its variant, Zhang et al. (2016b, 2019) found that the column CO performance
540 could be greatly improved by adjusting the BCON using the satellite observation. A similar
541 approach could be applied in future WRF-CMAQ simulations as well. Second, as pointed by
542 Heald et al. (2003), the regional emissions, especially biomass burning, could be a significant
543 source for elevated CO concentrations and thus underestimation of these emissions could

544 contribute to the CO underprediction. A more robust set of fire emissions from FINN generated
545 by NCAR based on satellite retrievals has been applied to the similar time period recently but
546 using the WRF-Chem model (Zhang and Wang, 2019) and were found to improve the column
547 CO performance. Last, Emmons et al. (2009) showed positive biases (i.e., 19%) of MOPITT
548 retrievals over the land when compared to in-situ measurements and the biases may have been
549 increasing over time due to the MOPITT bias drift (e.g., 0.5% yr⁻¹ for version 7 retrieval). The
550 predicted TOR can capture the observed high values over the eastern U.S. and oceans and the
551 low values in elevated terrain especially in summer and it shows the best performance among all
552 gas species. Both satellite observations and simulations can capture the elevated column NO₂
553 over the industrial and metropolitan areas in the domain where large nitrogen oxide (NO_x)
554 emission sources are located especially in winter. The model shows moderate underprediction
555 with an NMB of -27.8% in summer which can be attributed to both uncertainties in the emissions
556 and satellite retrievals. For example, the lightning emissions of NO_x are missing from this study,
557 which have been found by previous studies (Allen et al., 2012) to contribute up to 2.0×10^{15}
558 molecules cm⁻² over the southern U.S., the Gulf of Mexico, and northern Atlantic Ocean during
559 the summer. Boersma et al. (2004) also found that different column NO₂ retrieval approaches
560 may lead to large errors (> 25%) over polluted areas. Column HCHO over the CONUS
561 especially the southeastern U.S. is well predicted in summer in terms of both magnitude and
562 spatial distribution and correlates well with the biogenic emission source regions. The
563 underprediction of column HCHO in winter may indicate potential underestimation of
564 anthropogenic emissions. Other reasons including potential low yield of HCHO from isoprene
565 and terpene in the CB05 mechanism and uncertainties in satellite retrievals (Stavrakou et al.,
566 2009; Lorente et al., 2017). For example, According to Stavrakou et al. (2009), the air mass

567 factors used for HCHO column calculation may bear ~18% error under clear sky conditions to
568 ~50% error for very cloudy conditions. The winter typically has higher cloud cover than summer
569 (See Figs. 6 and 7) and thus higher uncertainties for HCHO column.

570 **3.2.4 Simulated O₃ and PM_{2.5} exceedances of NAAQS levels**

571 National Ambient Air Quality Standards (NAAQS) are set for criteria pollutants,
572 including O₃ and PM_{2.5}, to provide protection against adverse health and welfare effects
573 (www.epa.gov/criteria-air-pollutants/naaqs-table). In this section, the average number of days
574 per year where the 24-hr PM_{2.5} NAAQS level (35 µg m⁻³) and the max 8-h O₃ NAAQS level (70
575 ppb) are exceeded from the WRF-CMAQ predictions is compared with the number of
576 exceedances in the monitoring data (i.e., O₃ from AQS and CASTNET and PM_{2.5} from
577 IMPROVE and CSN). This comparison is intended to better characterize the ability of the model
578 to simulate the high-concentration days that could be especially relevant in regulatory
579 assessments. In Figure 14, the five-year average of the annual number of exceedance days is
580 shown for WRF-CMAQ and the monitoring data at monitor locations. As shown, the
581 observations indicate a large number of annual exceedance days for max 8-h O₃ over major
582 cities, especially in CA, TX, the Midwest, and northeastern U.S. The spatial distribution of the
583 observed number of exceedance days from the AQS and CASTNET networks aligns well with
584 the nonattainment map reported by the Green Book of U.S. EPA ([https://www.epa.gov/green-](https://www.epa.gov/green-book)
585 [book](https://www.epa.gov/green-book)). The WRF-CMAQ model also captures the distribution of the number of exceedance days
586 very well, especially in CA and northeastern U.S. The domain-average values of NMB, NME,
587 and R are -3.4%, 14.0%, and 0.98, respectively, also indicating a good performance. For PM_{2.5},
588 the largest number of exceedance days based on the IMPROVE and CSN observations mainly
589 occurs in the northwestern U.S., Midwest, and major cities in the northeastern U.S. The number

590 of exceedance days is generally much lower for PM_{2.5} than O₃. The spatial distribution of the
591 number of exceedance days for observed PM_{2.5} aligns well with nonattainment areas reported by
592 the Green Book from U.S. EPA in CA. However, the number of simulated PM_{2.5} exceedance
593 days underpredicts the observation-based values in the western U.S. mainly due to large
594 underpredictions of PM_{2.5} concentrations in the same areas as shown in Figure 10. The
595 simulation better predicts the distribution of the number of exceedance days in the eastern U.S.
596 where terrain is relatively flat and wildfire less prevalent. The domain-average values of NMB,
597 NME, and R are -29.0%, 80.8%, and 0.21, respectively.

598 **4. Impacts of chemistry-meteorology feedbacks**

599 In this section, the impacts of chemistry-meteorology feedbacks including aerosol direct
600 and indirect effects on regional meteorology and air quality over the U.S. are further examined
601 by comparing results from two-way WRF-CMAQ and offline coupled WRF and CMAQ. Model
602 performance from the two sets of simulations is first compared to demonstrate the potential
603 performance improvements of the two-way model, and the impacts on regional meteorology and
604 air quality are further investigated via the spatial difference plots for selected variables and
605 species.

606 **4.1 Meteorology**

607 Figures 2 and 8 compare observations and simulations from the two-way WRF-CMAQ
608 and WRF-only models for precipitation and SWCF/LWCF, respectively. Tables 1 and 2 also
609 summarize the model performance statistics for all major meteorological variables for the two
610 simulations. The statistics of some cloud variables from the WRF-only simulation are not
611 available due to missing model outputs. Overall, good performance is evident for both

612 simulations for surface meteorological variables with slightly better performance for most of
613 variables (except for RH2 in both seasons and T2 in summer) for the two-way WRF-CMAQ
614 simulation than the WRF-only simulation. The MBs for the two-way WRF-CMAQ vs. WRF-
615 only simulation are 1.1 °C vs 1.2 °C for T2, 2.2% vs 2.1% for RH2, 0.57 m s⁻¹ vs 0.58 m s⁻¹ for
616 WS10, 16.7 degree vs 16.9 degree for WD10, and 0.05-0.71 mm day⁻¹ vs 0.04-0.72 mm day⁻¹ for
617 precipitation in winter and -1.1 °C vs -0.9 °C for T2, 3.7% vs 3.2% for RH2, 0.38 m s⁻¹ vs 0.42
618 m s⁻¹ for WS10, 49.1 degree vs 49.8 degree for WD10, and 0.13-0.75 mm day⁻¹ vs 0.19-0.9 mm
619 day⁻¹ for precipitation in summer. The spatial distributions for SWCF and LWCF are better
620 captured in both seasons especially over the eastern U.S., Atlantic Ocean, and Gulf of Mexico in
621 winter and over the Midwest and Pacific Northwest in summer. Compared to WRF-only, two-
622 way WRF-CMAQ shows noticeably better performance in terms of both MB and RMSE for
623 radiation and cloud forcing, with MBs of 11.3 vs. 19.5 W m⁻² for SWDOWN, 7.5 vs 14.1 W m⁻²
624 for GSW, -0.9 vs. -6.3 W m⁻² for GLW, 4.0 vs. 4.7 W m⁻² for OLR, -3.0 vs. -7.4 W m⁻² for
625 SWCF, and -3.3 vs. -4.1 W m⁻² for LWCF in winter and with MBs of 43.6 vs. 59.4 W m⁻² for
626 SWDOWN, 33.6 vs 47.2 W m⁻² for GSW, -13.4 vs. -16.8 W m⁻² for GLW, 2.3 vs. 3.0 W m⁻² for
627 OLR, -22.8 vs. -31.1 W m⁻² for SWCF, and -8.6 vs. -9.0 W m⁻² for LWCF in summer. These
628 results are consistent with those reported by Yahya et al. (2015a,b) that showed similar
629 improvements in meteorological and radiative variables when comparing predictions from WRF-
630 Chem with those from WRF only. Since identical inputs and physics options are used in both
631 simulations, the differences in performance for meteorological variables is due to the
632 consideration of feedback processes among chemistry, aerosol, cloud, and radiation in the two-
633 way coupled WRF-CMAQ simulation.

634 Figure 15 shows the 5-year average difference plots of selected major meteorological
635 variables including SWDOWN, T2, RH2, WS10, PBL height, and precipitation between two-
636 way WRF-CMAQ and WRF-only in 2008-2012. As shown, the incoming shortwave radiation is
637 reduced by up to 24.8 W m^{-2} (13.6%) with a domain-average of 13.0 W m^{-2} (6%) due to the
638 combined aerosol direct and indirect radiative effects over the domain. The reduction is
639 predominant over the eastern U.S. where both aerosol loading and cloud cover are high and over
640 the oceans where cloud cover is high. The magnitude of shortwave radiation reduction in this
641 work is consistent with other studies. For example, Wang et al. (2015a) found that the combined
642 aerosol direct and indirect effects using the WRF/Chem model, which includes the sub-scale
643 cloud forcing not treated in the current WRF-CMAQ model, may decrease the incoming
644 shortwave radiation by 16.0 W m^{-2} in the summer over the U.S. Hogrefe et al. (2015) reported
645 the reduction of shortwave radiation may reach up to 20 W m^{-2} over the eastern U.S. by only
646 considering the aerosol direct effect using an older version of WRF-CMAQ v5.0.1. Xing et al.
647 (2015b) showed that the aerosol direct forcing may cause the surface shortwave radiation to
648 decrease by up to 10 W m^{-2} over the eastern U.S. over a decadal time period using WRF-CMAQ
649 v5.0. The reduction of shortwave radiation further reduces the surface temperature by up to
650 $0.25 \text{ }^{\circ}\text{C}$ over the eastern U.S., which is much larger than the reduction of $0.1 \text{ }^{\circ}\text{C}$ reported by
651 Hogrefe et al. (2015), mainly due to the inclusion of aerosol indirect effects. However there are
652 smaller reductions of T2 over the Pacific Ocean and even increases (by up to $0.1 \text{ }^{\circ}\text{C}$) over large
653 areas of Atlantic Ocean and Gulf of Mexico where much larger reductions of shortwave radiation
654 occur. As pointed by Wang et al. (2015a), due to the much larger heat capacity of ocean, the
655 response of sea surface temperature is less sensitive to the change of shortwave radiation for
656 ocean compared to the land. The large increase of incoming longwave radiation and latent heat

657 (figures not shown) caused by the aerosol indirect effects and other complex feedback processes
658 over the ocean compensates for the reduction of shortwave radiation, especially over the Atlantic
659 Ocean and Gulf of Mexico, and thus leads to less reduction or even increases of T2. RH2 is
660 found to mostly increase by 3.4% over the land caused by the decrease of temperature while
661 decrease by 2.6% over the ocean caused by either the increase of temperature or large decrease
662 of water vapor. Over the land, the decreases in shortwave radiation and temperature along with
663 the latent heat (figure not shown) lead to a more stable PBL and thus suppress the wind (by
664 reducing the wind speed as shown). Over the ocean, the changes lead to a more unstable PBL
665 and thus enhance the wind over the ocean. The wind speed and PBL height are reduced by up to
666 0.05 m s^{-1} and 25 m, respectively, over the U.S. The aerosol feedbacks on precipitation are also
667 mixed with relatively large decreases by up to 0.4 mm day^{-1} over the U.S. and increases by up to
668 0.4 mm day^{-1} over oceans. The suppression of precipitation over the land is mainly due to the
669 formation of more small sized CCNs caused by aerosol indirect effects and align well with areas
670 with high aerosol loadings while the enhancement of precipitation, especially along coastlines
671 and over oceans, might be associated with the larger CCN formation via more activated sea-salt
672 particles as indicated by Zhang et al. (2010) and Wang et al. (2015a).

673 **4.2 Air Quality**

674 Figures 9-11 compare observations and simulations from two-way WRF-CMAQ and
675 offline CMAQ for O_3 , $\text{PM}_{2.5}$, and $\text{PM}_{2.5}$ constituents. Tables 3 and 4 summarize the statistics for
676 all major chemical variables for the two simulations. As shown in Figure 9, two-way WRF-
677 CMAQ shows better performance for both the monthly variation of O_3 (throughout the whole
678 year) over AQS sites and the diurnal pattern of O_3 (especially during winter) over CASTNET
679 sites due to better performance of T2 and radiation compared to offline WRF and CMAQ. As

680 shown in Figure 10, two-way WRF-CMAQ shows better spatial distribution of PM_{2.5} in winter
681 and similar one in summer and better performance for PM_{2.5} for most of months over CSN sites
682 and for cold seasons across IMPROVE sites compared to offline CMAQ. Figure 11 shows
683 systematically better performance for SO₄²⁻, NO₃⁻, NH₄⁺, and TC with more data within 1:2 or
684 closer to 1:1 ratio lines of scatter plots in both seasons. Overall, as shown in Tables 3 and 4, both
685 simulations show generally good performance for all major chemical species except for PM₁₀.
686 For example., the domain-average NMBs are 10.6% (AQS) and -3.0% (CASTNET) vs. 14.2%
687 (AQS) and 0.2% (CASTNET) for O₃ in summer, -7.2% (CSN) and 8.6% (IMPROVE) vs. 1.8%
688 (CSN) and 23.7% (IMPROVE) for PM_{2.5} in winter and -13.2% (CSN) and -26.9% (IMPROVE)
689 vs. -14.0% (CSN) and -22.8% (IMPROVE) for PM_{2.5} in summer for two-way WRF-CMAQ and
690 offline-coupled CMAQ, respectively. The two-way WRF-CMAQ shows better domain-wide
691 statistics in terms of both correlation and biases for many variables including O₃, SO₄²⁻, NO₃⁻,
692 and EC as well as TOR and column NO₂ in both seasons, apparently due to the treatment of
693 chemistry-meteorology feedbacks. Offline CMAQ performs better for total PM_{2.5} especially in
694 the western U.S. due to higher dust emissions from higher wind speed and higher SOA due to
695 stronger radiation and higher temperature. However more robust comparisons are needed in the
696 future with improved dust emissions and the use of FINN wildfire emissions.

697 Figure 16 shows the 5-year average difference plots of selected chemical variables
698 including CO, O₃, NO_x, volatile organic compounds (VOCs), SO₄²⁻, SOA, PM_{2.5}, and PM₁₀
699 between two-way WRF-CMAQ and offline-coupled CMAQ. As shown, the CO mixing ratios
700 decrease by up to 79.2 ppb (27.8%) especially over the western U.S. with a domain-average
701 reduction of 3.0 ppb (3.1%) due to reduced formation of CO from the oxidation of VOCs caused
702 by reduced solar radiation as indicated by Zhang et al. (2017). Such reductions seem to dominate

703 over the increases caused by reduced PBL height, especially in the western U.S. where PBL
704 height reductions are minimum. The O₃ mixing ratios decrease by up to 5.2 ppb (16.2%) with
705 domain-average of 1.7 ppb (4.2%) mainly due to the reduced solar radiation and T2. The change
706 of O₃ is consistent with other studies such as Makar et al. (2015) and Wang et al. (2015a) that
707 also reported lower O₃ mixing ratios caused by aerosol direct and indirect effects. On the other
708 hand, both NO_x and VOC mixing ratios increase over the eastern U.S. while they decrease over
709 the western U.S. The increase should be caused by the combination of the large reduction of PBL
710 mixing and reduced solar radiation which reduces NO₂ photolysis and VOC oxidation to SOA.
711 For aerosol species, SO₄²⁻ concentrations increase by up to 0.38 μg m⁻³ (26.6%) especially over
712 the eastern U.S. In fact, the decrease of O₃ mixing ratios caused by feedbacks is expecting to
713 reduce SO₄²⁻ production via the gas-phase oxidation pathway due to the influence of O₃ on OH,
714 but increase SO₄²⁻ production via the aqueous-phase chemistry pathway due to more clouds in
715 the two-way WRF-CMAQ simulation. Thus, the net increase of SO₄²⁻ is more dominate by the
716 aqueous-phase chemistry instead of the gas-phase oxidation. This net increase of SO₄²⁻, in turn,
717 leads to an increase of NH₄⁺ and decrease of NO₃⁻ (figures not shown) through aerosol
718 thermodynamic equilibrium. SOA concentrations decrease by up to 0.34 μg m⁻³ (41.6%)
719 especially over the eastern U.S. due to the large reduction of oxidants. PM_{2.5} concentrations also
720 decrease by up to 5.2 μg m⁻³ (49.1%) with a domain-average of 0.34 μg m⁻³ (8.6%), and PM₁₀
721 concentrations decrease by up to 19.3 μg m⁻³ (64.8%) with a domain-average of 1.1 μg m⁻³
722 (11.1%). The reductions are more apparent over the western U.S. than the eastern U.S. partially
723 due to the compensation of the increase of SO₄²⁻ and NH₄⁺ and decrease of other secondary
724 aerosols over the eastern U.S., as well as the relatively large reduction of dust concentrations
725 over the western U.S. caused by reduced wind speed.

726 5. Summary and conclusion

727 In this study, two sets of long-term simulations for 2008-2012 using the two-way coupled
728 WRF-CMAQ and offline coupled WRF and CMAQ, respectively, are conducted, evaluated, and
729 compared to investigate the performance improvements due to chemistry-meteorology feedbacks
730 and impacts of those feedbacks on the regional air quality in the U.S. First, the two-way coupled
731 WRF-CMAQ simulation with both aerosol direct and indirect radiative forcing is
732 comprehensively evaluated in both winter and summer seasons and the annual trend is examined
733 between observations and simulations for selected major variables. The results show that WRF-
734 CMAQ performs well for major surface meteorological variables such as temperature at 2 m,
735 relative humidity at 2 m, wind speed at 10 m, and precipitation with domain-average MBs of -
736 1.1-1.1 °C, 2.2-3.7%, 0.38-0.57 m s⁻¹, and 0.13-0.23 mm day⁻¹ (except for 0.71-0.75 mm day⁻¹
737 against NCDC), respectively, in winter and summer. The relatively large positive biases for
738 precipitation are found to be more apparent when observed precipitation is low (dominated more
739 by the non-convective precipitation) and are thus believed to be more associated with
740 uncertainties in the Morrison microphysics scheme. The long-term simulation also shows
741 generally good performance for major radiation and cloud radiative variables. Relatively large
742 model biases still exist for cloud variables such as CDNC, COT, and CWP, indicating that the
743 processes associated with aerosol indirect effects are still not well understood and an accurate
744 simulation of those effects is still challenging using state-of-the-science models. WRF-CMAQ
745 can also capture the observed year-to-year variations well for almost all the major meteorological
746 and chemical variables.

747 Two-way WRF-CMAQ also shows generally good or acceptable performance for max 8-
748 h O₃, PM_{2.5} and PM_{2.5} constituents, with NMBs generally within ±15% for O₃ and ±30% for

749 PM_{2.5} species. For example, the domain-average NMBs are 10.6 % and -3.0 % for max 8-h O₃
750 against AQS and CASTNET in summer and -13.2 to -7.2 % and -26.9 to 8.6 % for PM_{2.5} against
751 CSN and IMPROVE in both seasons. O₃ mixing ratios are overpredicted for most months,
752 especially in the winter, in part due to the larger overprediction of T2 during the cold season. The
753 overall model biases are small for PM_{2.5} due to the compensation of relatively large
754 underpredictions of SO₄²⁻ and OC, especially in the warm season, and overprediction of NO₃⁻ in
755 the cold season. In addition to biases inherited from the meteorology, the model performance for
756 chemistry also suffers from uncertainties associated with emissions, the use of a coarse spatial
757 resolution, and representation of aerosol formation pathways in the model. For example, the
758 relatively large biases for EC might be associated with poorly allocated anthropogenic/wildfire
759 emissions and those for OC might be due to underestimation of SOA formation in version 5.0.2
760 of CMAQ. WRF-CMAQ also predicts the column abundances of chemical species well and the
761 relatively large model biases for CO are found to be associated with an underestimation of
762 BCONs. The model better reproduces the observed number of exceedance days for O₃ than
763 PM_{2.5} mainly due to better performance for O₃ than PM_{2.5} concentrations.

764 The performance comparison between two-way WRF-CMAQ and WRF-only simulations
765 shows that two-way WRF-CMAQ model performs better for major surface meteorological,
766 radiation, and cloud radiative variables due to the consideration of chemistry-meteorology
767 feedbacks associated with aerosol direct and indirect forcing. The feedbacks are found to reduce
768 the 5-year average SWDOWN by up to 24.8 W m⁻², T2 by up to 0.25 °C, PBL height by up to 25
769 m, wind speed by up to 0.05 m s⁻¹, and precipitation by up to 0.4 mm day⁻¹ over the CONUS,
770 which in turn affect the air quality significantly. As a result of feedbacks, two-way WRF-CMAQ
771 outperforms offline CMAQ for O₃, SO₄²⁻, NO₃⁻, NH₄⁺, and EC as well as TOR and column NO₂

772 in terms of both spatiotemporal variations and domain-average statistics due to better
773 meteorology performance for variables such as T2, WS10, radiation, and precipitation. Despite
774 these improvements, the offline CMAQ performs better for total PM_{2.5} in terms of domain-
775 average statistics, which could be partially caused by the compensation of larger under- and
776 over-predictions of PM_{2.5} constituents. More robust comparison for PM_{2.5} should be performed
777 with improved dust and wildfire emissions in future work. Chemistry-meteorology feedbacks are
778 found to play important roles in affecting U.S. air quality by reducing domain-wide 5-year
779 average surface CO by 3.0 ppb (3.1%) and up to 79.2 ppb (27.8%), O₃ by 1.7 ppb (4.1%) and up
780 to 5.2 ppb (16.2%), PM_{2.5} by 0.34 μg m⁻³ (8.6%) and up to 5.2 μg m⁻³ (49.1%), and PM₁₀ by 1.1
781 μg m⁻³ (11.1%) and up to 19.3 μg m⁻³ (64.8%) mainly due to reduction of radiation, temperature,
782 and wind speed.

783 In summary, the two-way coupled WRF-CMAQ modeling in this study shows generally
784 satisfactory and consistent performance for the long-term prediction of regional meteorology and
785 air quality when compared to other studies in the literature. Possible causes for the
786 meteorological and chemical biases that were identified through this work can provide valuable
787 information for future model development to improve the two-way coupled WRF-CMAQ model
788 and those biases should also be considered when making future climate/air quality projections.
789 Non-negligible model improvements for many major meteorological and chemical variables
790 compared to the traditional application of offline coupled WRF and CMAQ suggest the
791 importance of chemistry-meteorology feedbacks, especially aerosol direct and indirect effects.
792 The feedbacks should be considered along with other factors in developing future model
793 applications to inform policy making.

794 **Code Availability**

795 The modeling system used in this study is based on the 2-way coupled WRF-CMAQ model
796 derived from WRF v3.4 and CMAQ v5.0.2. Relevant code for CMAQ v5.0.2, its coupling to
797 WRF and aerosol direct feedbacks are publicly available from: doi:10.5281/zenodo.1079898.
798 WRF v3.4 code can be downloaded from
799 http://www2.mmm.ucar.edu/wrf/users/download/get_source.html. The version of the coupled
800 WRF-CMAQ model with the additional indirect aerosol forcing approach of Yu et al. (2014) can
801 be downloaded from the following website: <https://person.zju.edu.cn/shaocaiyu#674502>.

802 **Author contribution**

803 YZ and MB defined the scope of the manuscript. YZ and KW designed all the simulations. SY
804 and DW developed the two-way coupled WRF-CMAQ code. KW conducted all the simulations
805 and performed the analyses. KW drafted the manuscript. YZ, SY, DW, JP, RM, JK, and MB
806 reviewed and edited the manuscript.

807 **Competing interests**

808 The authors declare that they have no conflict of interest.

809 **Acknowledgements**

810 This work was developed at North Carolina State University and Northeastern University under
811 Assistance Agreement No. RD835871 awarded by the U.S. Environmental Protection Agency to
812 Yale University. The views expressed in this manuscript are those of the authors alone and do
813 not necessarily reflect the views and policies of the U.S. Environmental Protection Agency. EPA
814 does not endorse any products or commercial services mentioned in this publication. High
815 performance computing was support from Yellowstone (ark:/85065/d7wd3xhc) provided by

816 NCAR's CISL, sponsored by the NSF and the Stampede XSEDE high-performance computing
817 support under the NSF ACI-1053575. The work of S. Yu is supported by the Department of
818 Science and Technology of China (No. 2016YFC0202702, 2018YFC0213506 and
819 2018YFC0213503), National Research Program for Key Issues in Air Pollution Control in China
820 (No. DQGG0107) and National Natural Science Foundation of China (No. 21577126 and
821 41561144004). The authors gratefully acknowledge the availability of CERES, GPCP, MODIS,
822 MOPITT, NCDC, OMI, PRISM, SCHIAMACHY, and TMPA data. The authors thank Dr. Ralf
823 Bennartz from Vanderbilt University for providing the CDNC data. The authors also would like
824 to thank Drs. Jerry Herwehe and Shannon Koplitz from the U.S. EPA for their constructive and
825 very helpful comments.

826 **References**

- 827 Abdul-Razzak, H. and Ghan, S. J.: A parameterization of aerosol activation 2. Multiple aerosol
828 types, *J. Geophys. Res.*, 105 (D3), 6837-6844, 2000.
- 829 Alapaty, K., Herwehe, J. A., Otte, T. L., Nolte, C. G., Bullock, O. R., Mallard, M. S., Kain, J. S.,
830 and Dudhia, J.: Introducing subgrid-scale cloud feedbacks to radiation for regional
831 meteorological and climate modeling, *Geophys. Res. Lett.*, 39, L24809,
832 <https://doi.org/10.1029/2012GL054031>, 2012.
- 833 Allen, D. J., Pickering, K. E., Pinder, R. W., Henderson, B. H., Appel, K. W., and Prados, A.:
834 Impact of lightning-NO on eastern United States photochemistry during the summer of 2006 as
835 determined using the CMAQ model, *Atmos. Chem. Phys.*, 12, 1737-
836 1758, <https://doi.org/10.5194/acp-12-1737-2012>, 2012.
- 837 Appel, K. W., Gilliland, A. B., Sarwar, G., and Gilliam, R. C.: Evaluation of the Community
838 Multiscale Air Quality (CMAQ) model version 4.5: Sensitivities impacting model performance:
839 Part I, Ozone, *Atmos. Environ.*, 41, 9603-9615, 2007.
- 840 Appel, K. W., Pouliot, G. A., Simon, H., Sarwar, G., Pye, H. O. T., Napelenok, S. L., Akhtar, F.,
841 and Roselle, S. J.: Evaluation of dust and trace metal estimates from the Community Multiscale
842 Air Quality (CMAQ) model version 5.0, *Geosci. Model Dev.*, 6, 883-899,
843 <https://doi.org/10.5194/gmd-6-883-2013>, 2013.
- 844 Appel, K. W., Napelenok, S. L., Foley, K. M., Pye, H. O. T., Hogrefe, C., Luecken, D. J., Bash,
845 J. O., Roselle, S. J., Pleim, J. E., Foroutan, H., Hutzell, W. T., Pouliot, G. A., Sarwar, G., Fahey,

846 K. M., Gantt, B., Gilliam, R. C., Heath, N. K., Kang, D., Mathur, R., Schwede, D. B., Spero, T.
847 L., Wong, D. C., and Young, J. O.: Description and evaluation of the Community Multiscale Air
848 Quality (CMAQ) modeling system version 5.1, *Geosci. Model Dev.*, 10, 1703–1732,
849 <https://doi.org/10.5194/gmd-10-1703-2017>, 2017.

850 Baklanov, A., Schlünzen, K. H., Suppan, P., Baldasano, J., Brunner, D., Aksoyoglu, S.,
851 Carmichael, G., Douros, J., Flemming, J., Forkel, R., Galmarini, S., Gauss, M., Grell, G., Hirtl,
852 M., Joffre, S., Jorba, O., Kaas, E., Kaasik, M., Kallos, G., Kong, X., Korsholm, U., Kurganski,
853 A., Kushta, J., Lohmann, U., Mahura, A., Manders-Groot, A., Maurizi, A., Moussiopoulos, N.,
854 Rao, S. T., Savage, N., Seigneur, C., Sokhi, R. S., Solazzo, E., Solomos, S., Sørensen, B.,
855 Tsegas, G., Vignati, E., Vogel, B., and Zhang, Y.: Online coupled regional meteorology-
856 chemistry models in Europe: Current status and prospects, *Atmos. Chem. Phys.*, 14, 317–398,
857 [doi:10.5194/acp-14-317-2014](https://doi.org/10.5194/acp-14-317-2014), 2014.

858 Bennartz, R.: Global assessment of marine boundary layer cloud droplet number concentration
859 from satellite, *J. Geophys. Res.*, 112, D02201, <http://dx.doi.org/10.1029/2006JD007547>, 2007.

860 Boersma, K. F., Eskes, H. J., and Brinksma, E. J.: Error analysis for tropospheric NO₂ retrieval
861 from space, *J. Geophys. Res.*, 109, D04311, [doi:10.1029/2003JD003962](https://doi.org/10.1029/2003JD003962), 2004.

862 Brunner, D., Savage, N., Jorba, O., Eder, B., Giordano, L., Badia, A., Balzarini, A., Baro, R.,
863 Bianconi, R., Chemel, C., Curci, G., Forkel, R., Jimenez-Guerrero, P., Hirtl, M., Hodzic, A.,
864 Hozak, L., Im, U., Knote, C., Makar, P., Manders-Groot, A., van Meijgaard, E., Neal, L., Perez,
865 J. L., Pirovano, G., San Jose, R., Schroder, W., Sokhi, R. S., Syrakov, D., Torian, A., Tuccella,
866 P., Werhahn, J., Wolke, R., Yahya, K., Zabkar, R., Zhang, Y., Hogrefe, C., and Galmarini, S.:
867 Comparative analysis of meteorological performance of coupled chemistry-meteorology models
868 in the context of AQMEII phase 2, *Atmos. Environ.*, 115, 470–498,
869 [doi:10.1016/j.atmosenv.2014.12.032](https://doi.org/10.1016/j.atmosenv.2014.12.032), 2015.

870 Byun, D. W. and Schere K. L.: Review equations, computational algorithms, and other
871 components of the Models-3 Community Multi-Scale Air Quality (CMAQ) modeling system,
872 *Applied Mechanics Reviews*, 59(2), 51–77, [doi:10.1115/1.2128636](https://doi.org/10.1115/1.2128636), 2006.

873 Choi, M.W., Lee, J. H., Woo, J. W., Kim, C. H., and Lee, S. H.: Comparison of PM_{2.5} chemical
874 components over East Asia simulated by the WRF-Chem and WRF/CMAQ models: On the
875 models' prediction inconsistency, *Atmosphere*, 10, 618, 2019.

876 Cohen, A. E., Cavallo, S. M., Coniglio, M. C., and Brooks, H. E.: A review of planetary
877 boundary layer parameterization schemes and their sensitivity in simulating southeastern U.S.
878 cold season severe weather environments, *Weather and Forecasting*,
879 <https://doi.org/10.1175/WAF-D-14-00105.1>, 2015.

880 Dong, X., Fu, J. S., Huang, K., Tong, D., and Zhuang, G.: Model development of dust emission
881 and heterogeneous chemistry within the Community Multiscale Air Quality modeling system
882 and its application over East Asia, *Atmos. Chem. Phys.*, 16, 8157–8180,
883 <https://doi.org/10.5194/acp-16-8157-2016>, 2016.

884 Eder, B. and Yu, S.: A performance evaluation of the 2004 release of Models-3 CMAQ, *Atmos.*
885 *Environ.*, 40(26):4811–4824, 2006.

886 Emery, C., Liu, Z., Russell, A. G., Odman, M. T., Yarwood, G., and Kumar, N.:
887 Recommendations on statistics and benchmarks to assess photochemical model performance, J.
888 Air Waste Manage. Assoc., 67:5, 582-598, doi:10.1080/10962247.2016.1265027, 2017.

889 Emmons, L. K., Edwards, D. P., Deeter, M. N., Gille, J. C., Campos, T., Nédélec, P., Novelli, P.,
890 and Sachse, G.: Measurements of Pollution In The Troposphere (MOPITT) validation through
891 2006, Atmos. Chem. Phys., 9, 1795–1803, <https://doi.org/10.5194/acp-9-1795-2009>, 2009.

892 Gan, C.-M., Pleim, J., Mathur, R., Hogrefe, C., Long, C. N., Xing, J., Wong, D., Gilliam, R., and
893 Wei, C.: Assessment of long-term WRF–CMAQ simulations for understanding direct aerosol
894 effects on radiation "brightening" in the United States, Atmos. Chem. Phys., 15, 12193–12209,
895 <https://doi.org/10.5194/acp-15-12193-2015>, 2015a.

896 Gan, C.-M., Binkowski, F., Pleim, J., Xing, J., Wong, D., Mathur, R., and Gilliam, R.:
897 Assessment of the aerosol optics component of the coupled WRF–CMAQ model using CARES
898 field campaign data and a single column model, Atmos. Environ., 115, 670-682, 2015b.

899 Gantt, B., He, J., Zhang, X., Zhang, Y., and Nenes, A.: Incorporation of advanced aerosol
900 activation treatments into CESM/CAM5: model evaluation and impacts on aerosol indirect
901 effects, Atmos. Chem. Phys., 14, 7485–7497, <https://doi.org/10.5194/acp-14-7485-2014>, 2014.

902 Gantt, B., Sarwar, G., Xing, J., Simon, H., Schwede, D., Hutzell, W. T., Mathur, R., and Saiz-
903 Lopez, A.: The impact of iodide-mediated ozone deposition and halogen chemistry on surface
904 ozone concentrations across the continental United States, Environ. Sci. Technol., 51 (3), 1458-
905 1466, 2017.

906 Ghan, S. J., Laulainen, N. S., Easter, R. C., Wagener, R., Nemesure, S., Chapman, E. G., Zhang,
907 Y., and Leung, L. R.: Evaluation of aerosol direct radiative forcing in MIRAGE, J. Geophys.
908 Res., 106, 5295–5316, 2001.

909 Glotfelty, T., He, J., and Zhang, Y.: Impact of future climate policy scenarios on air quality and
910 aerosol-cloud interactions using an advanced version of CESM/CAM5: Part I. model evaluation
911 for the current decadal simulations, Atmos. Environ., 152, 222-239, 2017.

912 Grell, G. A., Peckham, S. E., Schmitz, R., McKenn, S. A., Frost, G., Skamarock, W. C., and
913 Eder, B.: Fully Coupled “Online” chemistry within the WRF Model, Atmos. Environ., 39, 6957–
914 6975, 2005.

915 Grell, G. A. and Baklanov, A.: Integrated modelling for forecasting weather and air quality: A
916 call for fully coupled approaches, Atmos. Environ., 45, 38, 6845–6851, 2011.

917 He, J. and Zhang, Y.: Improvement and further development in CESM/CAM5: Gasphase
918 chemistry and inorganic aerosol treatments, Atmos. Chem. Phys., 14, 9171-9200,
919 <http://dx.doi.org/10.5194/acp-14-9171-2014>, 2014.

920 Heald, C. L., Jacob, D. J., Fiore, A. M., Emmons, L. K., Gille, J. C., Deeter, M. N., Warner, J.,
921 Edwards, D. P., Crawford, J. H., Hamlin, A. J., Sachse, G. W., Browell, E. V., Avery, M. A.,
922 Vay, S. A., Westberg, D. J., Blake, D. R., Singh, H. B., Sandholm, S. T., Talbot, R. W., and
923 Fuelberg, H. E.: Asian outflow and trans-Pacific transport of carbon monoxide and ozone

924 pollution: An integrated satellite, aircraft, and model perspective, *J. Geophys. Res.*, 108(D24),
925 4804, doi:10.1029/2003JD003507, 2003.

926 Herwehe, J. A., Otte, T. L., Mathur, R., and Rao, S. T.: Diagnostic analysis of ozone
927 concentrations simulated by two regional-scale air quality models, *Atmos. Environ.*, 45, 5957–
928 5969, 2011.

929 Hogrefe, C., Pouliot, G., Wong, D., Torian, A., Roselle, S., Pleim, J., and Mathur, R.: Annual
930 application and evaluation of the online coupled WRF–CMAQ system over North America
931 under AQMEII phase 2, *Atmos. Environ.*, 115, 683–694, 2015.

932 Hong, C., Zhang, Q., Zhang, Y., Tang, Y., Tong, D., and He, K.: Multi-year downscaling
933 application of two-way coupled WRF v3.4 and CMAQ v5.0.2 over east Asia for regional climate
934 and air quality modeling: model evaluation and aerosol direct effects, *Geosci. Model Dev.*, 10,
935 2447–2470, <https://doi.org/10.5194/gmd-10-2447-2017>, 2017.

936 Hong, C.-P., Zhang, Q., Zhang, Y., Davis, S. J., Zhang, X., Tong, D., Guan, D., Liu, Z., and He,
937 K.-B.: Weakened aerosol radiative effects may mitigate the climate penalty on Chinese air
938 quality, *Nature Climate Change*, in press, 2020.

939 Iacono, M. J., Delamere, J. S., Mlawer, E. J., Shephard, M. W., Clough, S. A., and Collins, W.
940 D.: Radiative forcing by long-lived greenhouse gases: Calculations with the AER radiative
941 transfer models, *J. Geophys. Res. Atmos.*, 113, D13103, <https://doi.org/10.1029/2008JD009944>,
942 2008.

943 IPCC: Global warming of 1.5°C, An IPCC Special Report on the impacts of global warming of
944 1.5°C above pre-industrial levels and related global greenhouse gas emission pathways, in the
945 context of strengthening the global response to the threat of climate change, sustainable
946 development, and efforts to eradicate poverty edited by Masson-Delmotte, V., Zhai, P., Pörtner,
947 H. O., Roberts, D., Skea, J., Shukla, P. R., Pirani, A., Moufouma-Okia, W., Péan, C., Pidcock,
948 R., Connors, S., Matthews, J. B. R., Chen, Y., Zhou, X., Gomis, M. I., Lonnoy, E., Maycock, T.,
949 Tignor, M., and Waterfield, T., 2018.

950 Jacobson, M. Z., Lu, R., Turco, R. P., and Toon, O. B.: Development and application of a new
951 air pollution modeling system. Part I: Gas-phase simulations, *Atmos. Environ.*, 30B, 1939–1963,
952 1996.

953 Jacobson, M. Z.: GATOR-GCMM: A global- through urban-scale air pollution and weather
954 forecast model 1. Model design and treatment of subgrid soil, vegetation, roads, rooftops, water,
955 sea, ice, and snow, *J. Geophys. Res.*, 106, 5385–5401, 2001.

956 Jung, J., Souri, A. H., Wong, D. C., Lee, S., Jeon, W., Kim, J., and Choi, Y.: The impact of the
957 direct effect of aerosols on meteorology and air quality using aerosol optical depth assimilation
958 during the KORUS - AQ campaign, *J. Geophys. Res. Atmos.*, 124, 8303–8319,
959 <https://doi.org/10.1029/2019JD030641>, 2019.

960 Kain, J. S.: The Kain-Fritsch convective parameterization: An update, *J. Appl. Meteorol.*, 43,
961 170–181, [https://doi.org/10.1175/1520-0450\(2004\)043<0170:TKCPAU>2.0.CO;2](https://doi.org/10.1175/1520-0450(2004)043<0170:TKCPAU>2.0.CO;2), 2004.

962 Karydis, V. A., Tsimpidi, A. P., and Pandis, S. N.: Evaluation of a three-dimensional chemical
963 transport model (PMCAMx) in the eastern United States for all four seasons, *J. Geophys. Res.*,
964 112, D14211, doi:10.1029/2006JD007890, 2007.

965 Kaufman, Y. J., Smirnov, A., Holben, B., and Dubovik, O.: Baseline maritime aerosol
966 methodology to derive the optical thickness and scattering properties, *Geophys. Res. Lett.*, 28,
967 3251, doi:10.1029/2001GL013312, 2001.

968 Kelly, J., Koplitz, S., Baker, K., Holder, A., Pye, H., Murphy, B., Bash, J., Henderson, B.,
969 Possiel, N., Simon, H., Eyth, A., Jang, C., Phillips, S., and Timin, B.: Assessing PM_{2.5} model
970 performance for the conterminous U.S. with comparison to model performance statistics from
971 2007-2015, *Atmos. Environ.*, 214, <https://doi.org/10.1016/j.atmosenv.2019.116872>, 2019.

972 Kukkonen, J., Olsson, T., Schultz, D. M., Baklanov, A., Klein, T., Miranda, A. I., Monteiro, A.,
973 Hirtl, M., Tarvainen, V., Boy, M., Peuch, V.-H., Poupkou, A., Kioutsioukis, I., Finardi, S.,
974 Sofiev, M., Sokhi, R., Lehtinen, K. E. J., Karatzas, K., San José, R., Astitha, M., Kallos, G.,
975 Schaap, M., Reimer, E., Jakobs, H., and Eben, K.: A review of operational, regional-scale,
976 chemical weather forecasting models in Europe, *Atmos. Chem. Phys.*, 12, 1–87,
977 doi:10.5194/acp-12-1-2012, 2012.

978 Li, P., Wang, L., Guo, P., Yu, S., Mehmood, K., Wang, S., Liu, W., Seinfeld, J. H., Zhang, Y.,
979 Wong, D., Alapaty, K., Pleim, J., and Mathur, R.: High reduction of ozone and particulate matter
980 during the 2016 G-20 summit in Hangzhou by forced emission controls of industry and traffic,
981 *Environ. Chem. Lett.*, 15:709–715, doi:10.1007/s10311-017-0642-2, 2017.

982 Lin, M., Holloway, T., Carmichael, G. R., and Fiore, A. M.: Quantifying pollution inflow and
983 outflow over East Asia in spring with regional and global models, *Atmos. Chem. Phys.*, 10,
984 4221–4239, <https://doi.org/10.5194/acp-10-4221-2010>, 2010.

985 Liu, X.-H., Zhang, Y., Xing, J., Zhang, Q., Wang, K., Streets, D. G., Jang, C. J., Wang, W.-X.,
986 and Hao, J. M.: Understanding of regional air pollution over China using CMAQ:- Part II.
987 Process analysis and ozone sensitivity to precursor emissions, *Atmos. Environ.*, 44(20), 3719–
988 3727, 2010.

989 Lorente, A., Folkert Boersma, K., Yu, H., Dörner, S., Hilboll, A., Richter, A., Liu, M., Lamsal,
990 L. N., Barkley, M., De Smedt, I., Van Roozendaal, M., Wang, Y., Wagner, T., Beirle, S., Lin, J.-
991 T., Krotkov, N., Stammes, P., Wang, P., Eskes, H. J., and Krol, M.: Structural uncertainty in air
992 mass factor calculation for NO₂ and HCHO satellite retrievals, *Atmos. Meas. Tech.*, 10, 759–
993 782, <https://doi.org/10.5194/amt-10-759-2017>, 2017.

994 Ma, P.-L., Rasch, P. J., Fast, J. D., Easter, R. C., Gustafson Jr., W. I., Liu, X., Ghan, S. J., and
995 Singh, B.: Assessing the CAM5 physics suite in the WRF-Chem model: implementation,
996 resolution sensitivity, and a first evaluation for a regional case study, *Geosci. Model Dev.*, 7,
997 755–778, <https://doi.org/10.5194/gmd-7-755-2014>, 2014.

998 Makar, P., A., Gong, W., Hogrefe, C., Zhang, Y., Curci, G., Žabkar, R., Milbrandt, J., Im, U.,
999 Balzarini, A., Baró, R., Bianconi, R., Cheung, P., Forkel, R., Gravel, S., Hirtl, M., Honzak, L.,
1000 Hou, A., Jiménez-Guerrero, P., Langer, M., Moran, M. B., Pabla, B., Pérez, J. L., Pirovano, G.,

- 1001 San José, R., Tuccella, P., Werhahn, J., Zhang, J., and Galmarini, S.: Feedbacks between air
1002 pollution and weather, Part 2: Effects on chemistry, *Atmos. Environ.*, 115, 499-526, 2015.
- 1003 Mathur, R., Xiu, A., Coats, C., Alapaty, K., Shankar, U., and Hanna, A.: Development of an air
1004 quality modeling system with integrated meteorology, chemistry, and emissions, *Proc.*
1005 *Measurement of Toxic and Related Air Pollutants*, AWMA, Cary, NC, September, 1998.
- 1006 Mathur, R., Xing, J., Gilliam, R., Sarwar, G., Hogrefe, C., Pleim, J., Pouliot, G., Roselle, S.,
1007 Spero, T. L., Wong, D. C., and Young, J.: Extending the Community Multiscale Air Quality
1008 (CMAQ) modeling system to hemispheric scales: overview of process considerations and initial
1009 applications, *Atmos. Chem. Phys.*, 17, 12449-12474, 2017.
- 1010 Matsui, H., Koike, M., Kondo, Y., Takegawa, N., Kita, K., Miyazaki, Y., Hu, M., Chang, S.-Y.,
1011 Blake, D. R., Fast, J. D., Zaveri, R. A., Streets, D. G., Zhang, Q. and Zhu, T.: Spatial and
1012 temporal variations of aerosols around Beijing in summer 2006: Model evaluation and source
1013 apportionment, *J. Geophys. Res.*, 114, D00G13, doi:10.1029/2008JD010906, 2009.
- 1014 Mebust, M. R., Eder, B. K., Binkowski, F. S., and Roselle, S. J.: Models-3 Community
1015 Multiscale Air Quality (CMAQ) model aerosol component: 2. Model evaluation, *J. Geophys.*
1016 *Res.*, 108(D6), 4184, doi:10.1029/2001JD001410, 2003.
- 1017 Mehmood, K., Wu, Y., Wang, L., Yu, S., Li, P., Chen, X., Li, Z., Zhang, Y., Li, M., Liu, W.,
1018 Wang, Y., Liu, Z., Zhu, Y., Rosenfeld, D., and Seinfeld, J. H.: Relative effects of open biomass
1019 burning and open crop straw burning on haze formation over central and eastern China:
1020 modeling study driven by constrained emissions, *Atmos. Chem. Phys.*, 20, 2419–2443,
1021 <https://doi.org/10.5194/acp-20-2419-2020>, 2020.
- 1022 Morrison, H., Thompson, G., and Tatarskii, V.: Impact of cloud microphysics on the
1023 development of trailing stratiform precipitation in a simulated squall line: Comparison of one-
1024 and two-moment schemes, *Mon. Weather Rev.*, 137, 991–1007,
1025 <https://doi.org/10.1175/2008MWR2556.1>, 2009.
- 1026 Penrod, A., Zhang, Y., Wang, K., Wu, S.-Y., and Leung, R. L.: Impacts of future climate and
1027 emission changes on US air quality, *Atmos. Environ.*, 89, 533-547,
1028 doi:10.1016/j.atmosenv.2014.01.001, 2014.
- 1029 Pleim, J. E.: A combined local and nonlocal closure model for the atmospheric boundary layer.
1030 Part I: Model description and testing, *J. Appl. Meteorol. Clim.*,
1031 <https://doi.org/10.1175/JAM2539.1>, 2007.
- 1032 Pleim, J., Young, J., Wong, D., Gilliam, R., Otte, T., and Mathur, R.: Two-way coupled
1033 meteorology and air quality modeling, in *Air Pollution Modeling and its Application*, edited by
1034 C. Borrego and A. I. Miranda, XIX, NATO Science for Peace and Security Series, Series C:
1035 Environmental Security, Springer, Dordrecht, 2008.
- 1036 Pleim, J. E. and Gilliam, R.: An indirect data assimilation scheme for deep soil temperature in
1037 the Pleim–Xiu land surface model, *J. Appl. Meteorol. Clim.*, 48, 1362-1376, 2009.

- 1038 Pye, H. O. T., Murphy, B. N., Xu, L., Ng, N. L., Carlton, A. G., Guo, H., Weber, R., Vasilakos,
1039 P., Appel, K. W., Budisulistiorini, S. H., Surratt, J. D., Nenes, A., Hu, W., Jimenez, J. L.,
1040 Isaacman-VanWertz, G., Misztal, P. K., and Goldstein, A. H.: On the implications of aerosol
1041 liquid water and phase separation for organic aerosol mass, *Atmos. Chem. Phys.*, 17, 343–369,
1042 doi:10.5194/acp-17-343-2017, 2017.
- 1043 Pye, H. O. T., Nenes, A., Alexander, B., Ault, A. P., Barth, M. C., Clegg, S. L., Collett Jr., J. L.,
1044 Fahey, K. M., Hennigan, C. J., Herrmann, H., Kanakidou, M., Kelly, J. T., Ku, I.-T., McNeill, V.
1045 F., Riemer, N., Schaefer, T., Shi, G., Tilgner, A., Walker, J. T., Wang, T., Weber, R., Xing, J.,
1046 Zaveri, R. A., and Zuend, A.: The acidity of atmospheric particles and clouds, *Atmos. Chem.*
1047 *Phys.*, 20, 4809–4888, <https://doi.org/10.5194/acp-20-4809-2020>, 2020.
- 1048 Remer, L. A., Kaufman, Y. J., Tanré, D., Mattoo, S., Chu, D. A., Martins, J. V., Li, R. R.,
1049 Ichoku, C., Levy, R. C., and Kleidman, R. G.: The MODIS aerosol algorithm, products, and
1050 validation, *J. Atmos. Sci.*, 62, 947-973, 2005.
- 1051 Roy, B., Pouliot, G. A., Gilliland, A., Pierce, T., Howard, S., Bhave, P. V., and Benjey, W.:
1052 Refining fire emissions for air quality modeling with remotely sensed fire counts: A wildfire case
1053 study, *Atmos. Environ.*, 41(3), 655-665, doi:10.1016/j.atmosenv.2006.08.037, 2007.
- 1054 San Joaquin Valley Air Pollution Control District: 2018 Plan for the 1997, 2006, and 2012 PM_{2.5}
1055 Standards, November 15, 2018, <https://www.valleyair.org/pmplans>, 2018.
- 1056 Sarwar, G., Luecken, D., Yarwood, G., Whitten, G. Z., and Carter, W. P. L.: Impact of an
1057 updated carbon bond mechanism on predictions from the CMAQ modeling system: Preliminary
1058 assessment, *J. Appl. Meteor. Clim.*, 47, 3e14, 2008.
- 1059 Sarwar, G., Gantt, B., Schwede, D., Foley, K., Mathur, R., and Saiz-Lopez, A.: Impact of
1060 enhanced ozone deposition and halogen chemistry on tropospheric ozone over the Northern
1061 Hemisphere, *Environ. Sci. Technol.*, 49 (15), 9203-9211, 2015.
- 1062 Scheffe, R. D., Strum, M., Phillips, S. B., Thurman, J., Eyth, A., Fudge, S., Morris, M., Palma,
1063 T., and Cook, R.: Hybrid modeling approach to estimate exposures of hazardous air pollutants
1064 (HAPs) for the National Air Toxics Assessment (NATA), *Environ. Sci. Technol.*, 2016, 50(22),
1065 12356–12364, doi:10.1021/acs.est.6b04752, 2016.
- 1066 Schwede, D., Pouliot, G. A., and Pierce, T.: Changes to the biogenic emissions inventory system
1067 version 3 (BEIS3), in: Proceedings of the 4th CMAS Models-3 Users' Conference, Chapel Hill,
1068 NC, 26–28 September, 2005.
- 1069 Sekiguchi, A., Shimadera, H., and Kondo, A.: Impact of aerosol direct effect on wintertime
1070 PM_{2.5} simulated by an online coupled meteorology-air quality model over East Asia, *Aerosol.*
1071 *Air Qual. Res.*, 18, 1068–1079, 2018.
- 1072 Solazzo, E., Hogrefe, C., Colette, A., Garcia-Vivanco, M., and Galmarini, S.: Advanced error
1073 diagnostics of the CMAQ and Chimere modelling systems within the AQMEII3 model
1074 evaluation framework, *Atmos. Chem. Phys.*, 17, 10435-10465, 2017.

1075 Stavrakou, T., Müller, J.-F., De Smedt, I., Van Roozendael, M., van der Werf, G. R., Giglio, L.,
1076 and Guenther, A.: Global emissions of non-methane hydrocarbons deduced from SCIAMACHY
1077 formaldehyde columns through 2003–2006, *Atmos. Chem. Phys.*, 9, 3663–3679,
1078 doi:10.5194/acp-9-3663-2009, 2009.

1079 U.S. EPA: Our nation’s air status and trends through 2010, EPA-454/R-12-001, February 2012,
1080 https://www.epa.gov/sites/default/files/2017-11/documents/trends_brochure_2010.pdf, 2012.

1081 U.S. EPA: Policy assessment for the review of the National Ambient Air Quality Standards for
1082 particulate matter, EPA-452/R-20-002, January 2020,
1083 [https://www.epa.gov/sites/production/files/2020-](https://www.epa.gov/sites/production/files/2020-01/documents/final_policy_assessment_for_the_review_of_the_pm_naaqs_01-2020.pdf)
1084 [01/documents/final_policy_assessment_for_the_review_of_the_pm_naaqs_01-2020.pdf](https://www.epa.gov/sites/production/files/2020-01/documents/final_policy_assessment_for_the_review_of_the_pm_naaqs_01-2020.pdf), 2020.

1085 Vasilakos, P., Russell, A., Weber, R., and Nenes, A.: Understanding nitrate formation in a world
1086 with less sulfate. *Atmos. Chem. Phys.* 18, 12765-12775, 2018.

1087 Wang, K. and Zhang, Y.: Application, evaluation, and process analysis of U.S. EPA’s 2002
1088 multiple-pollutant air quality modeling platform, *Atmospheric and Climate Sciences*, 2, 254-289,
1089 2012.

1090 Wang, K. and Zhang, Y.: 3-D agricultural air quality modeling: Impacts of NH₃/H₂S gas-phase
1091 reactions and bi-directional exchange of NH₃, *Atmos. Environ.*, 98, 554-570, doi:
1092 10.1016/j.atmosenv.2014.09.010, 2014.

1093 Wang, K., Zhang, Y., Jang, C., Phillips, S., and Wang, B.: Modeling intercontinental air
1094 pollution transport over the trans-Pacific region in 2001 using the Community Multiscale Air
1095 Quality modeling system, *J. Geophys. Res.*, 114, D04307, doi:10.1029/2008JD010807, 2009.

1096 Wang, K., Zhang, Y., Nenes, A., and Fountoukis, C.: Implementation of dust emission and
1097 chemistry into the Community Multiscale Air Quality modeling system and initial application to
1098 an Asian dust storm episode, *Atmos. Chem. Phys.*, 12, 10209–10237,
1099 <https://doi.org/10.5194/acp-12-10209-2012>, 2012.

1100 Wang, J., Wang, S., Jiang, J., Ding, A., Zheng, M., Zhao, B., Wong, C.-D., Zhou, W., Zheng, G.,
1101 Wang, L., Pleim, J., and Hao, J.: Impact of aerosol–meteorology interactions on fine particle
1102 pollution during China’s severe haze episode in January 2013, *Environ. Res. Lett.*, 9,
1103 doi:10.1088/1748-9326/9/9/094002, 2014.

1104 Wang, K., Zhang, Y., Yahya, K., Wu, S.-Y., and Grell, G.: Implementation and initial
1105 application of new chemistry-aerosol options in WRF/Chem for simulating secondary organic
1106 aerosols and aerosol indirect effects for regional air quality, *Atmos. Environ.*, 115, 716-732,
1107 doi:10.1016/j.atmosenv.2014.12.007, 2015a.

1108 Wang, K., Yahya, K., Zhang, Y., Hogrefe, C., Pouliot, G., Knote, C., Hodzic, A., Jose, R. S.,
1109 Perez, J. L., Jiménez-Guerrero, P., Baro, R., Makar, P., and Bennartz, R.: A multi-model
1110 assessment for the 2006 and 2010 simulations under the Air Quality Model Evaluation
1111 International Initiative (AQMEII) Phase 2 over North America: Part II. Evaluation of column
1112 variable predictions using satellite data, *Atmos. Environ.*, 115, 1–17,
1113 10.1016/j.atmosenv.2014.07.044, 2015b.

- 1114 Wang, K., Zhang, Y., and Yahya, K.: Decadal application of WRF/Chem over the continental
1115 U.S.: Simulation design, sensitivity simulations, and climatological model evaluation, *Atmos.*
1116 *Environ.*, 118331, doi: 10.1016/j.atmosenv.2021.118331, 2021.
- 1117 West, J. J., Ansari, A. S., and Pandis, S. N.: Marginal PM_{2.5}: Nonlinear aerosol mass response to
1118 sulfate reductions in the Eastern United States, *J. Air Waste Manage. Assoc.*, 49, 1415-1424,
1119 <https://doi.org/10.1080/10473289.1999.10463973>, 1999.
- 1120 Wiedinmyer, C., Quayle, B., Geron, C., Belote, A., McKenzie, D., Zhang, X., O'Neill, S., and
1121 Wynne, K. K.: Estimating emissions from fires in North America for air quality modeling,
1122 *Atmos. Environ.*, 40(19): 3419–32, doi:10.1016/j.atmosenv.2006.02.010, 2006.
- 1123 Wielicki, B. A., Barkstrom, B. R., Harrison, E. F., Lee III, R. B., Smith, G. L., and Cooper, J. E.:
1124 Clouds and the Earth's Radiant Energy System (CERES): An earth observing system
1125 experiment, *B. Am. Meteorol. Soc.*, 77, 853–868, 1996.
- 1126 Wilczak, J. M., Djalalova, I., McKeen, S., Bianco, L., Bao, J.-W., Grell, G., Peckham, S.,
1127 Mathur, R., McQueen, J., and Lee, P.: Analysis of regional meteorology and surface ozone during
1128 the TexAQS II field program and an evaluation of the NMM-CMAQ and WRF-Chem air quality
1129 models, *J. Geophys. Res.*, 114, D00F14, 2009.
- 1130 Wong, D. C., Pleim, J., Mathur, R., Binkowski, F., Otte, T., Gilliam, R., Pouliot, G., Xiu, A.,
1131 Young, J. O., and Kang, D.: WRF-CMAQ two-way coupled system with aerosol feedback:
1132 Software development and preliminary results, *Geosci. Model Dev.*, 5, 299–312,
1133 <https://doi.org/10.5194/gmd-5-299-2012>, 2012.
- 1134 Xing, J., Mathur, R., Pleim, J., Hogrefe, C., Gan, C.-M., Wong, D. C., Wei, C., and Wang, J.: Air
1135 pollution and climate response to aerosol direct radiative effects: A modeling study of decadal
1136 trends across the northern hemisphere, *J. Geophys. Res. Atmos.*, 120, 12,221–12,236,
1137 doi:10.1002/2015JD023933, 2015a.
- 1138 Xing, J., Mathur, R., Pleim, J., Hogrefe, C., Gan, C.-M., Wong, D. C., and Wei, C.: Can a
1139 coupled meteorology–chemistry model reproduce the historical trend in aerosol direct radiative
1140 effects over the Northern Hemisphere?, *Atmos. Chem. Phys.*, 15, 9997–10018,
1141 <https://doi.org/10.5194/acp-15-9997-2015>, 2015b.
- 1142 Xing, J., Wang, J., Mathur, R., Pleim, J., Wang, S., Hogrefe, C., Gan, C.-M., Wong, D., and Hao,
1143 J.: Unexpected benefits of reducing aerosol cooling effects, *Environ. Sci. Technol.*, 50, 7527–
1144 7534, <https://doi.org/10.1021/acs.est.6b00767>, 2016.
- 1145 Xing, J., Wang, J., Mathur, R., Wang, S., Sarwar, G., Pleim, J., Hogrefe, C., Zhang, Y., Jiang, J.,
1146 Wong, D. C., and Hao, J.: Impacts of aerosol direct effects on tropospheric ozone through
1147 changes in atmospheric dynamics and photolysis rates, *Atmos. Chem. Phys.*, 17, 9869–9883,
1148 <https://doi.org/10.5194/acp-17-9869-2017>, 2017.
- 1149 Xiu, A. and Pleim, J. E.: Development of a land surface model. Part I: Application in a
1150 mesoscale meteorological model, *J. Appl. Meteorol.*, 40, 192–209, [https://doi.org/10.1175/1520-0450\(2001\)040<0192:doalsm>2.0.co;2](https://doi.org/10.1175/1520-0450(2001)040<0192:doalsm>2.0.co;2), 2001.

- 1152 Yahya, K., Wang, K., Gudoshava, M., Glotfelty, T., and Zhang, Y.: Application of WRF/Chem
1153 over North America under the AQMEII Phase 2. Part I. Comprehensive evaluation of 2006
1154 simulation, *Atmos. Environ.*, 115, 733-755, doi:10.1016/j.atmosenv.2014.08.063, 2015a.
- 1155 Yahya, K., Wang, K., Zhang, Y., and Kleindienst, T. E.: Application of WRF/Chem over North
1156 America under the AQMEII Phase 2 – Part 2: Evaluation of 2010 application and responses of
1157 air quality and meteorology–chemistry interactions to changes in emissions and meteorology
1158 from 2006 to 2010, *Geosci. Model Dev.*, 8, 2095–2117, [https://doi.org/10.5194/gmd-8-2095-](https://doi.org/10.5194/gmd-8-2095-2015)
1159 2015, 2015b.
- 1160 Yahya, K., Wang, K., Campbell, P., Glotfelty, T., He, J., and Zhang, Y.: Decadal evaluation of
1161 regional climate, air quality, and their interactions over the continental US and their interactions
1162 using WRF/Chem version 3.6.1, *Geosci. Model Dev.*, 9, 671–695, [https://doi.org/10.5194/gmd-](https://doi.org/10.5194/gmd-9-671-2016)
1163 9-671-2016, 2016.
- 1164 Yarwood, G., Rao, S., Yocke, M., and Whitten, G. Z.: Final Report–Updates to the Carbon Bond
1165 Chemical Mechanism: CB05, Rep.RT-04-00675, Yocke and Co., Novato, Calif., 246 pp., 2005.
- 1166 Yoo, J.-W., Jeon, W., Park, S.-Y., Park, C., Jung, J., Lee, S.-H., and Lee, H. W.: Investigating
1167 the regional difference of aerosol feedback effects over South Korea using the WRF-CMAQ
1168 two-way coupled modeling system, *Atmos. Environ.*, 218, 116968, 2019.
- 1169 Yu, S., Eder, B., Dennis, R., Chu, S., and Schwartz, S.: New unbiased symmetric metrics for
1170 evaluation of air quality models, *Atmos. Sci. Lett.*, 7, 26-34, 2006.
- 1171 Yu, S. C., Mathur, R., Schere, K., Kang, D., Pleim, J., and Otte, T. L.: A detailed evaluation of
1172 the Eta-CMAQ forecast model performance for O₃, its related precursors, and meteorological
1173 parameters during the 2004 ICARTT Study, *J. Geophys. Res.*, 112, D12S14,
1174 doi:10.1029/2006JD007715, 2007.
- 1175 Yu, S. C., Mathur, R., Pleim, J., Wong, D., Carlton, A. G., Roselle, S., and Rao, S. T.:
1176 Simulation of the indirect radiative forcing of climate due to aerosols by the two-way coupled
1177 WRF-CMAQ over the eastern United States, in *Air Pollution Modeling and its Applications*,
1178 edited by D. G. Steyn and S. T. Castellì, XXI, Springer Netherlands, Netherlands, C(96), 579–
1179 583, 2011.
- 1180 Yu, S., Mathur, R., Pleim, J., Wong, D., Gilliam, R., Alapaty, K., Zhao, C., and Liu, X.: Aerosol
1181 indirect effect on the grid-scale clouds in the two-way coupled WRF–CMAQ: Model
1182 description, development, evaluation and regional analysis, *Atmos. Chem. Phys.*, 14, 11247–
1183 11285, <https://doi.org/10.5194/acp-14-11247-2014>, 2014.
- 1184 Yu, S., Li, P., Wang, L., Wu, Y., Wang, S., Liu, W., Zhu, T., Zhang, Y., Hu, M., Alapaty, K.,
1185 Wong, D., Pleim, J., Mathur, R., Rosenfeld, D., and Seinfeld, J.: Mitigation of severe urban haze
1186 pollution by a precision air pollution control approach, *Scientific Reports*, 8:8151,
1187 doi:10.1038/s41598-018-26344-1, 2018.
- 1188 Yu, X.-Y., Lee, T., Ayres, B., Kreidenweis, S. M., Malm, W., and Collett, J. L.: Loss of fine
1189 particle ammonium from denuded nylon filters, *Atmos. Environ.*, 40, 4797-4807, 2006.

1190 Zender, C. S., H. Bian, and D. Newman: Mineral Dust Entrainment and Deposition (DEAD)
1191 model: Description and 1990s dust climatology, *J. Geophys. Res.*, 108, 4416,
1192 doi:10.1029/2002JD002775, 2003.

1193 Zhang, Y.: Online coupled meteorology and chemistry models: History, current status, and
1194 outlook, *Atmos. Chem. Phys.*, 8, 2895-2932, doi:10.5194/acp-8-2895-2008, 2008.

1195 Zhang, Y. and Wang, Y.: Climate-driven ground-level ozone extreme in the fall over the
1196 Southeast United States, *P. Natl. Acad. Sci. USA*, 113, 10025–10030,
1197 <https://doi.org/10.1073/pnas.1602563113>, 2016.

1198 Zhang, Y. and Wang, K.: Project 3 - Air quality and climate modeling: Multi-model application,
1199 evaluation, intercomparison, and ensemble over the U.S., poster presentation at the Air Climate
1200 Energy (ACE) Centers Meeting, Pittsburgh, PA, June 18-19, 2019.

1201 Zhang, K. M., Knipping, E. M., Wexler, A. S., Bhave, P. V., and Tonnesen, G. S.: Size
1202 distribution of sea-salt emissions as a function of relative humidity, *Atmos. Environ.*, 39, 3373-
1203 3379, 2005.

1204 Zhang, Y., Liu, P., Pun, B, and Seigneur, C.: A comprehensive performance evaluation of MM5-
1205 CMAQ for the summer 1999 Southern Oxidants Study episode, Part-I. Evaluation protocols,
1206 databases and meteorological predictions, *Atmos. Environ.*, 40, 4825-4838,
1207 doi:10.1016/j.atmosenv.2005.12.043, 2006.

1208 Zhang, Y., Vijayaraghavan, K., Wen, X.-Y., Snell, H. E., and Jacobson, M. Z.: Probing into
1209 regional ozone and particulate matter pollution in the United States: 1. A 1-year CMAQ
1210 simulation and evaluation using surface and satellite data, *J. Geophys. Res.*, 114, D22304,
1211 doi:10.1029/2009JD011898, 2009a.

1212 Zhang, Y., Wen, X.-Y., Wang, K., Vijayaraghavan, K., and Jacobson, M. Z.: Probing into
1213 regional ozone and particulate matter pollution in the United States: 2. An examination of
1214 formation mechanisms through a process analysis technique and sensitivity study, *J. Geophys.*
1215 *Res.*, 114, D22305, doi:10.1029/2009JD011900, 2009b.

1216 Zhang, Y., Wen, X.-Y., and Jang C. J.: Simulating chemistry-aerosol-cloud-radiation-climate
1217 feedbacks over the continental US using the online-coupled Weather Research Forecasting
1218 Model with chemistry (WRF/Chem), *Atmos. Environ.*, 44(29), 3568-3582, doi:
1219 10.1016/j.atmosenv.2010.05.056, 2010.

1220 Zhang, Y., Sartelet, K., Zhu, S., Wang, W., Wu, S.-Y., Zhang, X., Wang, K., Tran, P., Seigneur,
1221 C., and Wang, Z.-F.: Application of WRF/Chem-MADRID and WRF/Polyphemus in Europe –
1222 Part 2: Evaluation of chemical concentrations and sensitivity simulations, *Atmos. Chem. Phys.*,
1223 13, 6845–6875, <https://doi.org/10.5194/acp-13-6845-2013>, 2013.

1224 Zhang, Y., Chen, Y., Fan, J., and Leung, L. R.: Application of an online-coupled regional
1225 climate model, WRF-CAM5, over East Asia for examination of ice nucleation schemes: Part II.
1226 Sensitivity to ice nucleation parameterizations and dust emissions, *Climate*, 3(3), 753-774,
1227 doi:10.3390/cli3030753, 2015a.

- 1228 Zhang, Y., Zhang, X., Wang, K., He, J., Leung, L. R., Fan, J.-W., and Nenes, A.: Incorporating
1229 an advanced aerosol activation parameterization into WRF-CAM5: Model evaluation and
1230 parameterization intercomparison, *J. Geophys. Res.*, 120 (14), doi:10.1002/2014JD023051,
1231 2015b.
- 1232 Zhang, Y., Zhang, X., Wang, L., Zhang, Q., Duan, F., and He, K.: Application of WRF/Chem
1233 over East Asia: Part I. Model evaluation and intercomparison with MM5/CMAQ, *Atmos.*
1234 *Environ.*, 124, 285–300, 2016a.
- 1235 Zhang, Y., Hong, C.-P., Yahya, K., Li, Q., Zhang, Q., and He, K.-B.: Comprehensive evaluation
1236 of multi-year real-time air quality forecasting using an online-coupled meteorology-chemistry
1237 model over southeastern United States, *Atmos. Environ.*, 138, 162-182,
1238 doi:10.1016/j.atmosenv.2016.05.006, 2016b.
- 1239 Zhang, Y., Wang, K., and He J.: Multi-year application of WRF-CAM5 over East Asia-Part II:
1240 Interannual variability, trend analysis, and aerosol indirect effects, *Atmos. Environ.*, 165, 222-
1241 239, 2017.
- 1242 Zhang, Y., Jena, C., Wang, K., Paton-Walsh, C., Guérette, E.-A., Utembe, S., Silver, J. D., and
1243 Keywood, M.: Multiscale applications of two online-coupled meteorology-chemistry models
1244 during recent field campaigns in Australia, Part I: Model description and WRF/Chem-ROMS
1245 evaluation using surface and satellite data and sensitivity to spatial grid resolutions, *Atmosphere*,
1246 10(4), 189, doi:10.3390/atmos10040189, 2019.
- 1247 Zheng, B., Zhang, Q., Zhang, Y., He, K. B., Wang, K., Zheng, G. J., Duan, F. K., Ma, Y. L., and
1248 Kimoto, T.: Heterogeneous chemistry: a mechanism missing in current models to explain
1249 secondary inorganic aerosol formation during the January 2013 haze episode in North China,
1250 *Atmos. Chem. Phys.*, 15, 2031–2049, <https://doi.org/10.5194/acp-15-2031-2015>, 2015.

Table 1. The 5-year average performance statistics for meteorological variables between two-way WRF-CMAQ and WRF-only simulations in winter, 2008-2012.

Variables	Datasets	Mean Obs	Two-way WRF-CMAQ				WRF-only					
			Mean Sim	R	MB	NMB (%)	RMSE	Mean Sim	R	MB	NMB (%)	RMSE
T2 (°C)	NCDC	7.5	8.6	0.97	1.1	14.9	1.6	8.6	0.97	1.2	15.8	1.6
RH2 (%)		72.9	75.1	0.79	2.2	3.0	6.3	75.0	0.79	2.1	2.8	6.3
WS10 (m s ⁻¹)		3.93	4.50	0.4	0.57	14.6	1.17	4.50	0.4	0.58	14.6	1.17
WD10 (deg)		166.4	183.1	0.0	16.7	10.0	44.2	183.3	0.0	16.9	10.2	44.4
Precipitation (mm day ⁻¹)	NCDC	1.54	2.25	0.46	0.71	46.3	1.94	2.26	0.47	0.72	47.0	1.94
	NADP	2.48	2.68	0.77	0.2	8.0	1.14	2.69	0.77	0.21	8.6	1.14
	GPCP	1.81	2.04	0.80	0.23	12.8	1.03	2.04	0.80	0.23	12.8	1.02
	PRISM	1.91	2.08	0.89	0.17	9.0	0.79	2.09	0.89	0.18	9.4	0.79
	TMPA	2.02	2.07	0.81	0.05	2.4	1.01	2.06	0.81	0.04	2.0	1.02
SWDOWN (W m ⁻²)	CERES	108.5	119.8	0.99	11.3	10.4	13.7	128.0	0.98	19.5	17.9	22.2
GSW (W m ⁻²)		87.1	94.6	0.99	7.5	8.6	10.1	101.3	0.98	14.1	16.2	17.1
GLW (W m ⁻²)		278.9	278.0	0.99	-0.9	-0.3	5.9	272.7	0.99	-6.3	-2.2	8.6
OLR (W m ⁻²)		222.3	226.2	0.99	4.0	1.8	5.1	227.0	0.99	4.7	2.1	5.8
SWCF (W m ⁻²)		-26.6	-23.6	0.91	-3.0	-11.1	6.3	-19.2	0.85	-7.4	-27.8	10.6
LWCF (W m ⁻²)		22.0	18.7	0.76	-3.3	-15.1	6.0	18.0	0.72	-4.1	-18.4	6.7
AOD	MODIS	0.11	0.04	0.44	-0.06	-59.8	0.08	N/A	N/A	N/A	N/A	N/A
CF		0.66	0.59	0.87	-0.07	-10.4	0.1	N/A	N/A	N/A	N/A	N/A
CDNC (cm ⁻³)		172.3	30.4	0.21	-141.9	-82.4	157.5	N/A	N/A	N/A	N/A	N/A
CWP (g m ⁻²)		177.4	97.0	0.63	-80.4	-45.3	93.2	N/A	N/A	N/A	N/A	N/A
COT		16.9	3.3	0.74	-13.6	-80.8	14.2	N/A	N/A	N/A	N/A	N/A

*outputs of AOD, CF, CDNC, CWP, and COT are not available from WRF-only simulations

Table 2. The 5-year average performance statistics for meteorological variables between two-way WRF-CMAQ and WRF-only simulations in summer, 2008-2012.

Variables	Datasets	Mean Obs	Two-way WRF-CMAQ				WRF-only					
			Mean Sim	R	MB	NMB (%)	RMSE	Mean Sim	R	MB	NMB (%)	RMSE
T2 (°C)	NCDC	22.3	22.2	0.95	-1.1	-4.6	1.7	22.4	0.95	-0.9	-3.7	1.6
RH2 (%)		67.0	70.7	0.91	3.7	5.5	6.6	70.1	0.91	3.2	4.7	6.3
WS10 (m s ⁻¹)		3.19	3.57	0.36	0.38	11.8	0.99	3.61	0.35	0.42	13.1	1.01
WD10 (deg)		146.4	195.4	0.0	49.1	33.5	67.3	196.1	0.0	49.8	34.0	67.9
Precipitation (mm day ⁻¹)	NCDC	2.11	2.86	0.5	0.75	35.6	1.93	3.01	0.5	0.9	42.6	2.01
	NADP	2.82	2.99	0.83	0.17	5.9	0.87	3.14	0.83	0.32	11.2	0.93
	GPCP	2.55	2.78	0.80	0.23	9.0	1.19	2.86	0.80	0.30	11.9	1.21
	PRISM	2.35	2.55	0.89	0.20	8.4	0.69	2.65	0.89	0.30	12.9	0.73
TMPA	2.70	2.83	0.80	0.13	4.8	1.27	2.89	0.81	0.19	6.8	1.27	
SWDOWN (W m ⁻²)	CERES	254.7	298.3	0.84	43.6	17.1	46.6	314.1	0.73	59.4	23.3	62.8
GSW (W m ⁻²)		222.5	256.1	0.75	33.6	15.1	37.6	269.7	0.57	47.2	21.2	51.7
GLW (W m ⁻²)		372.2	358.8	0.98	-13.4	-3.6	15.3	355.4	0.98	-16.8	-4.5	18.7
OLR (W m ⁻²)		257.2	259.6	0.96	2.3	0.9	4.8	260.2	0.96	3.0	1.2	5.2
SWCF (W m ⁻²)		-55.1	-32.3	0.69	-22.8	-41.3	27.6	-24.0	0.50	-31.1	-56.4	36.2
LWCF (W m ⁻²)		26.1	17.5	0.85	-8.6	-33.0	9.8	17.1	0.87	-9.0	-34.6	10.0
AOD	MODIS	0.20	0.07	0.67	-0.13	-67.8	0.14	N/A	N/A	N/A	N/A	N/A
CF		0.53	0.41	0.81	-0.12	-23.0	0.16	N/A	N/A	N/A	N/A	N/A
CDNC (cm ⁻³)		138.9	28.9	0.11	-110.0	-79.2	124.1	N/A	N/A	N/A	N/A	N/A
CWP (g m ⁻²)		162.2	54.6	0.65	-107.6	-66.3	113.8	N/A	N/A	N/A	N/A	N/A
COT		14.2	2.3	0.73	-11.9	-83.6	12.2	N/A	N/A	N/A	N/A	N/A

*outputs of AOD, CF, CDNC, CWP, and COT are not available from WRF-only simulations

Table 3. The 5-year average performance statistics for chemical variables between two-way WRF-CMAQ and offline CMAQ simulations in winter, 2008-2012.

Variables	Datasets	Mean Obs	Two-way WRF-CMAQ					Offline CMAQ				
			Mean Sim	R	MB	NMB (%)	NME (%)	Mean Sim	R	MB	NMB (%)	NME (%)
Max 8-hr O ₃ (ppb)	AQS	32.4	39.6	0.61	7.2	22.5	23.0	42.3	0.65	9.9	30.7	30.9
	CASTNET	34.9	36.6	0.76	1.7	4.9	9.4	39.7	0.75	4.7	13.5	14.3
PM _{2.5} (µg m ⁻³)	CSN	11.4	10.6	0.21	-0.8	-7.2	29.3	11.7	0.2	0.21	1.8	31.0
	IMPROVE	3.59	3.90	0.83	0.31	8.6	30.3	4.44	0.86	0.85	23.7	32.1
PM ₁₀ (µg m ⁻³)	AQS	19.9	12.7	0.04	-7.2	-36.3	46.9	15.7	0.17	-4.2	-21.3	42.8
	CSN	2.06	1.06	0.78	-1.0	-48.3	48.4	1.02	0.78	-1.04	-50.7	50.8
SO ₄ ²⁻ (µg m ⁻³)	IMPROVE	0.79	0.49	0.95	-0.3	-37.4	38.9	0.49	0.95	-0.3	-38.5	39.9
	CSN	2.37	2.36	0.79	-0.01	-0.3	25.8	2.89	0.81	0.52	21.7	37.8
NO ₃ ⁻ (µg m ⁻³)	IMPROVE	0.73	0.83	0.87	0.1	13.3	40.9	1.06	0.90	0.33	44.6	54.4
	CSN	1.30	0.92	0.80	-0.38	-29.4	30.5	1.03	0.81	-0.27	-21.0	24.1
EC (µg m ⁻³)	CSN	0.69	0.75	0.18	0.06	8.7	58.5	0.79	0.24	0.1	14.2	58.0
	IMPROVE	0.17	0.23	0.80	0.06	40.8	59.2	0.25	0.84	0.09	53.4	65.6
OC (µg m ⁻³)	IMPROVE	0.65	0.74	0.65	0.09	13.0	55.7	0.8	0.67	0.15	23.1	56.4
	CSN	3.05	3.27	0.01	0.22	7.2	53.2	3.49	0.0	0.44	14.4	55.8
TC (µg m ⁻³)	IMPROVE	0.53	0.62	0.75	0.09	17.5	51.3	0.68	0.78	0.15	28.1	52.6
	CSN	3.05	3.27	0.01	0.22	7.2	53.2	3.49	0.0	0.44	14.4	55.8
Col. CO (10 ¹⁸ mole. cm ⁻³)	MOPITT	1.96	1.56	0.70	-0.4	-20.5	21.6	1.57	0.69	-0.39	-19.8	21.1
	OMI	26.4	27.6	0.78	1.2	4.7	14.0	28.0	0.19	1.6	5.9	14.3
Col. NO ₂ (10 ¹⁵ mole. cm ⁻³)	SCIAMACHY	1.55	1.55	0.86	0.04	0.3	33.5	1.53	0.87	-0.02	-1.2	33.1
Col. HCHO (10 ¹⁵ mole. cm ⁻³)	SCIAMACHY	4.87	2.48	0.29	-2.39	-49.0	50.1	2.53	0.28	-2.34	-48.0	49.2

Table 4. The 5-year average performance statistics for chemical variables between two-way WRF-CMAQ and offline CMAQ simulations in summer, 2008-2012.

Variables	Datasets	Mean Obs	Two-way WRF-CMAQ					Offline CMAQ				
			Mean Sim	R	MB	NMB (%)	NME (%)	Mean Sim	R	MB	NMB (%)	NME (%)
Max 8-hr O ₃ (ppb)	AQS	47.9	53.0	0.66	5.1	10.6	13.2	54.8	0.66	6.8	14.2	15.6
	CASTNET	47.2	45.8	0.66	-1.4	-3.0	11.5	47.3	0.68	0.1	0.2	10.5
PM _{2.5} (µg m ⁻³)	CSN	11.4	9.9	0.74	-1.5	-13.2	20.5	9.8	0.71	-1.6	-14.0	20.8
	IMPROVE	6.19	4.52	0.88	-1.66	-26.9	31.2	4.78	0.86	-1.41	-22.8	28.9
PM ₁₀ (µg m ⁻³)	AQS	26.7	14.5	0.03	-12.2	-45.8	50.7	16.2	0.07	-10.5	-39.4	48.6
	CSN	2.86	2.57	0.91	-0.29	-10.2	15.1	2.34	0.91	-0.52	-18.1	19.5
SO ₄ ²⁻ (µg m ⁻³)	IMPROVE	1.40	1.11	0.98	-0.29	-20.9	21.3	1.08	0.98	-0.31	-22.5	22.6
	CSN	0.49	0.71	0.54	0.22	45.2	70.6	0.77	0.59	0.28	57.2	76.8
NO ₃ ⁻ (µg m ⁻³)	IMPROVE	0.20	0.19	0.6	-0.01	-4.7	71.4	0.22	0.63	0.02	10.3	72.2
	CSN	0.91	0.94	0.86	0.03	3.3	22.4	0.88	0.85	-0.03	-3.6	20.1
EC (µg m ⁻³)	CSN	0.56	0.79	0.56	0.23	41.0	56.3	0.79	0.55	0.23	41.9	55.5
	IMPROVE	0.20	0.24	0.56	0.04	20.4	58.8	0.26	0.52	0.06	27.9	63.0
OC (µg m ⁻³)	IMPROVE	1.37	0.70	0.31	-0.67	-49.2	54.0	0.75	0.28	-0.62	-45.4	52.4
	CSN	2.85	2.17	0.54	-0.67	-23.6	29.3	2.19	0.5	-0.65	-22.9	29.7
TC (µg m ⁻³)	IMPROVE	0.88	0.61	0.56	-0.27	-30.5	47.6	0.66	0.53	-0.23	-25.6	47.6
	MOPITT	1.82	1.32	0.75	-0.5	-27.8	27.8	1.32	0.54	-0.5	-27.3	27.3
Col. CO (10 ¹⁸ mole. cm ⁻³)	OMI	35.0	32.2	0.87	-2.8	-8.0	9.0	32.4	0.85	-2.6	-7.3	8.6
Col. NO ₂ (10 ¹⁵ mole. cm ⁻³)	SCIAMACHY	1.08	0.78	0.81	-0.3	-27.8	38.0	0.78	0.80	-0.3	-27.5	38.1
Col. HCHO (10 ¹⁵ mole. cm ⁻³)	SCIAMACHY	5.81	6.71	0.82	0.9	15.0	22.5	6.82	0.82	1.01	17.4	23.5

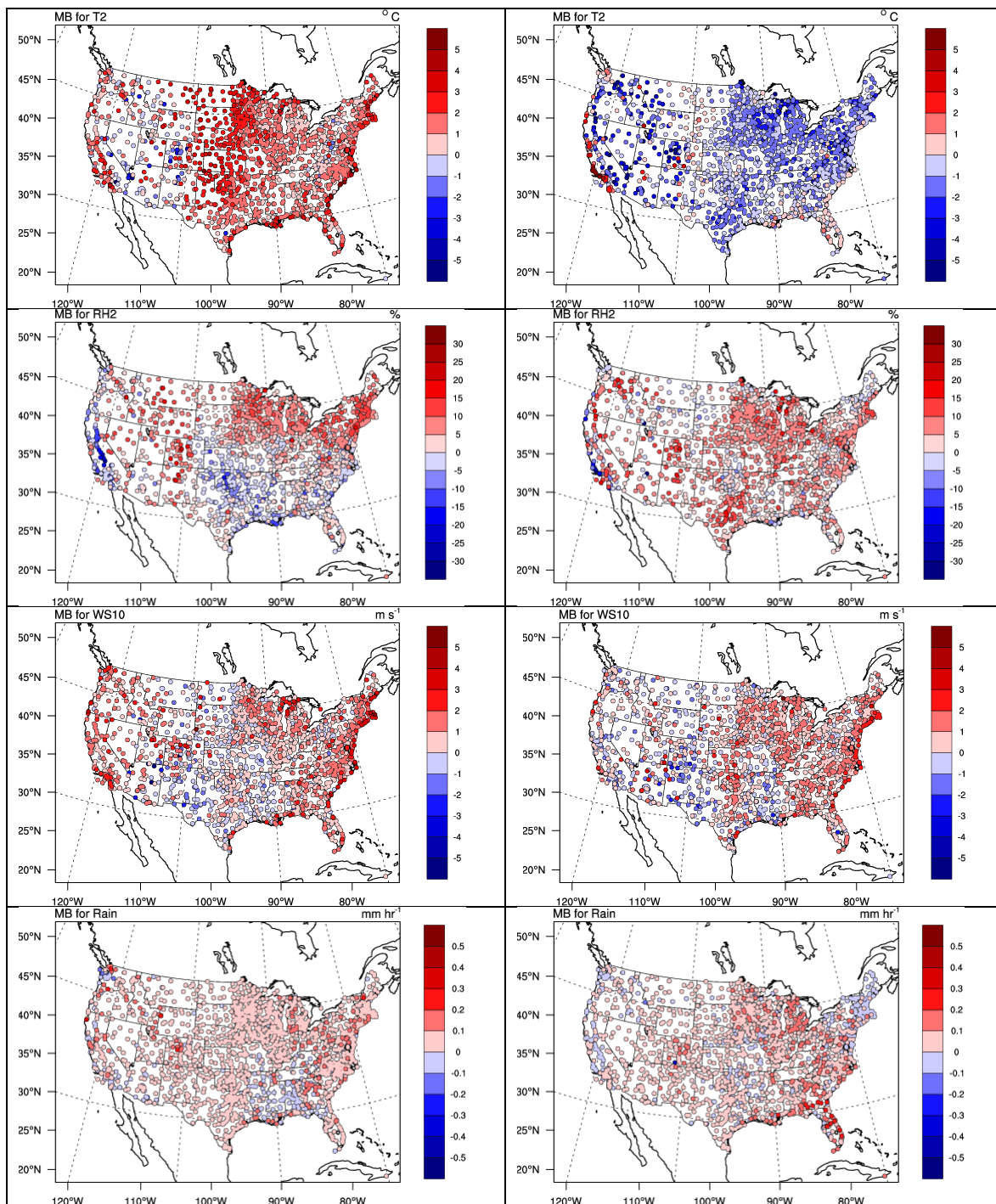


Figure 1. Spatial distributions of 5-year average MBs for 2-m temperature (T2), 2-m relative humidity (RH2), 10-m wind speed (WS10), and hourly precipitation from NCDc for two-way WRF-CMAQ in winter (left panel) and summer (right panel), 2008-2012.

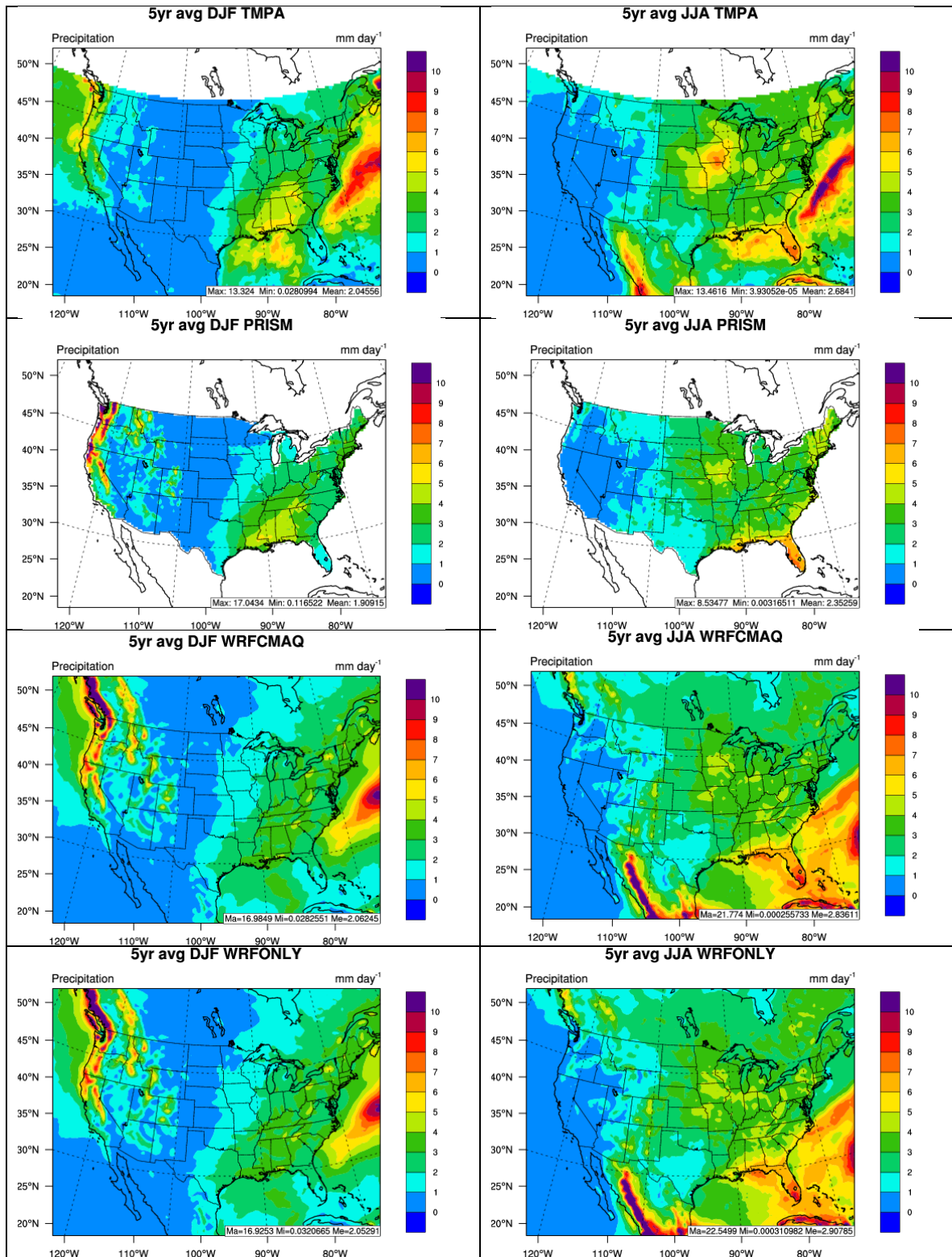


Figure 2. Spatial distributions of 5-year average of daily precipitation from TMPA, PRISM, two-way WRF-CMAQ, and WRF-only (from top to bottom) in winter (left panel) and summer (right panel), 2008-2012.

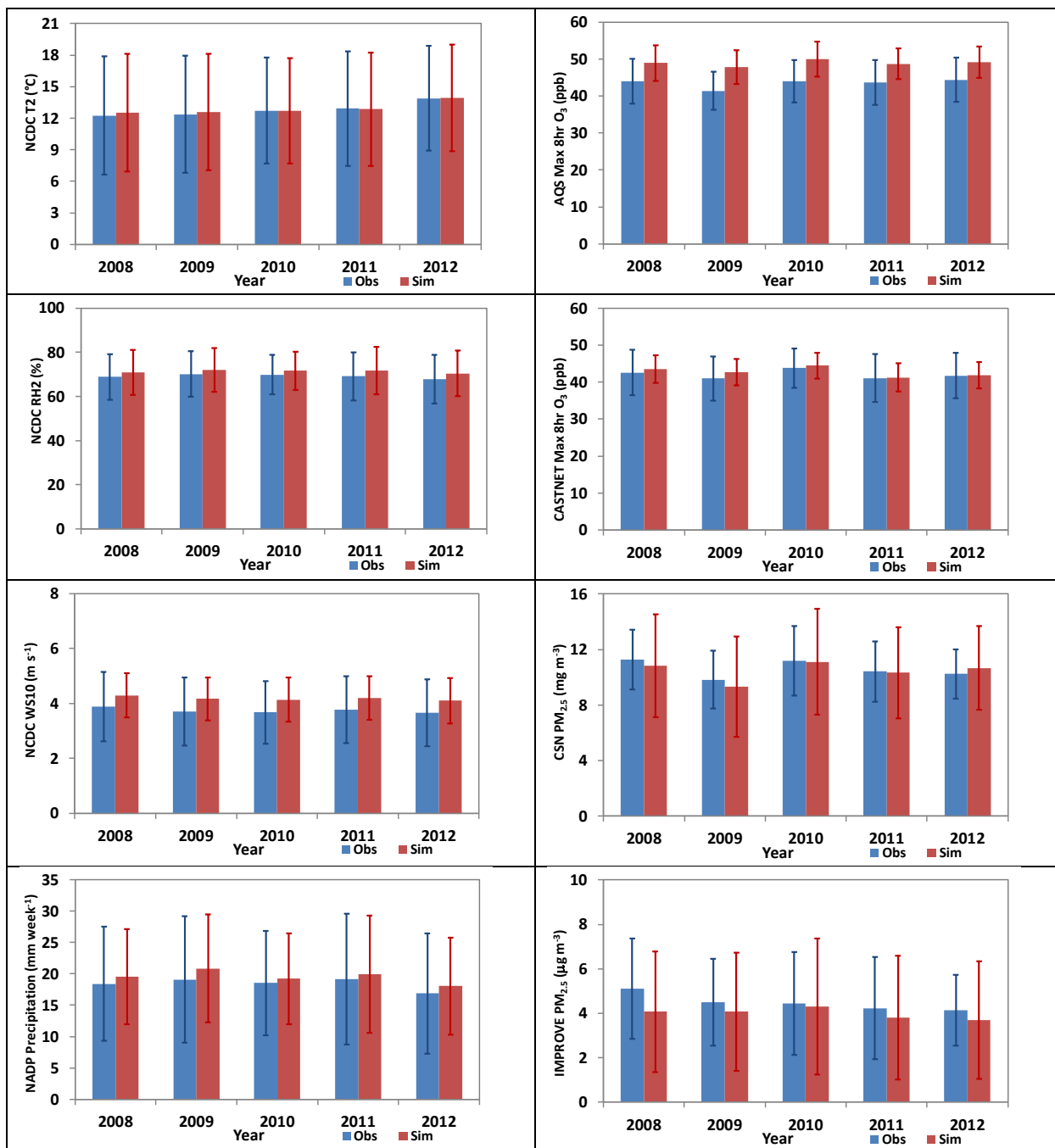


Figure 3. Bar charts for annual average observations and simulations (standard deviations are displayed as the error bars) from two-way WRF-CMAQ for major meteorological variables (left panel) and chemical species (right panel) in 2008-2012.

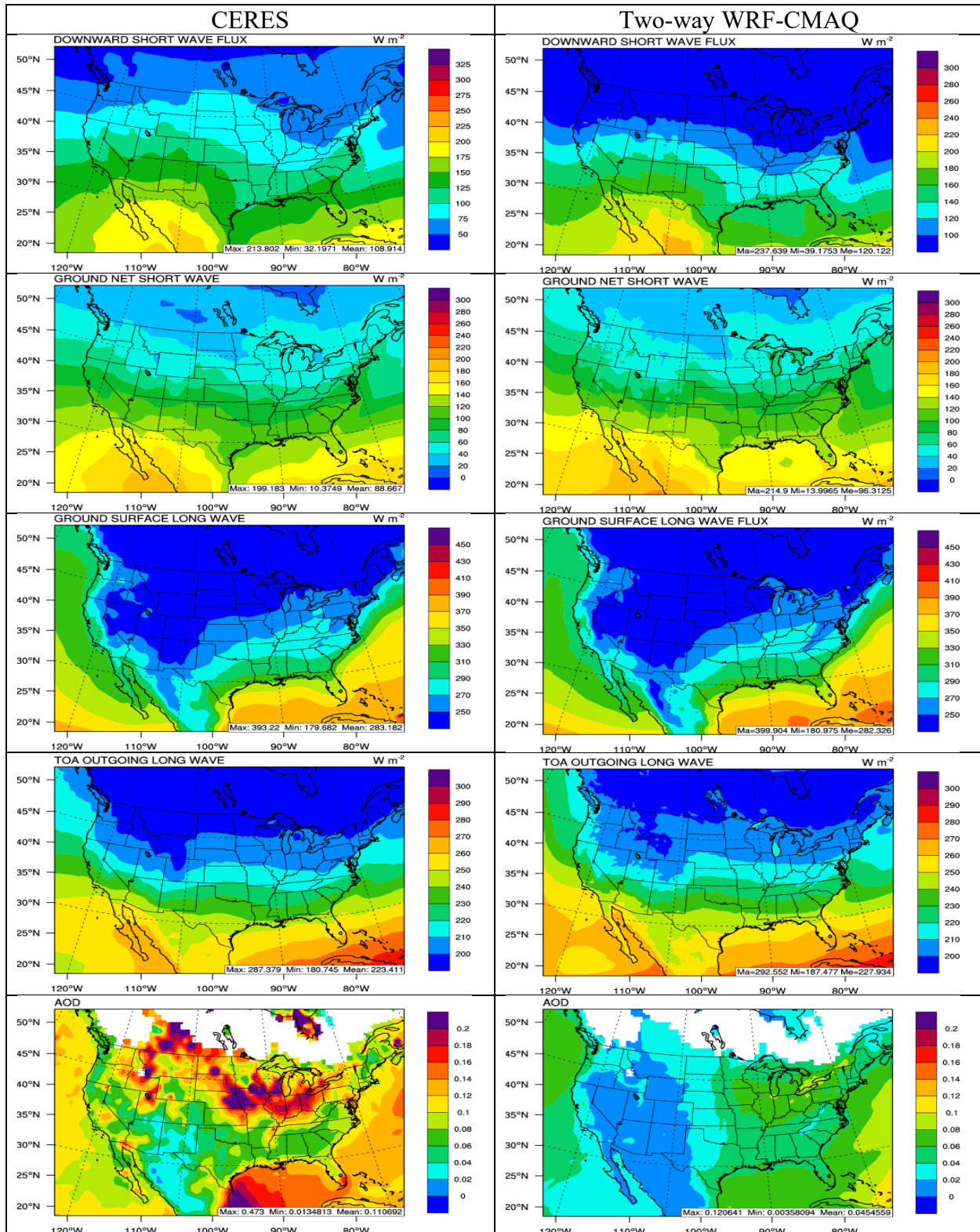


Figure 4. Spatial distribution of 5-year average major radiation variables (from top to bottom: SWDOWN, GSW, GLW, OLR, and AOD) between CERES observations (left panel) vs. two-way WRF-CMAQ (right panel) in winter, 2008-2012.

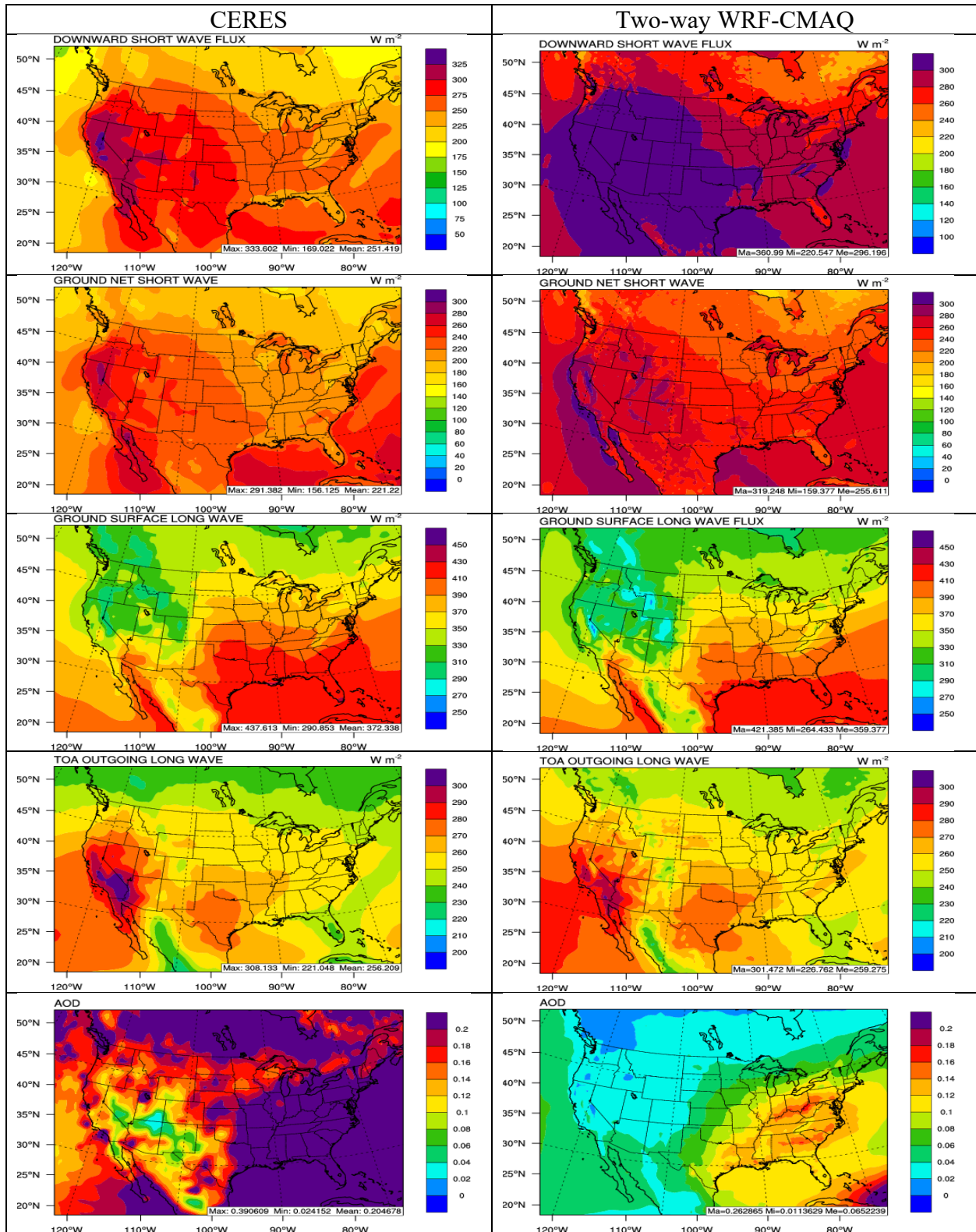


Figure 5. Spatial distribution of 5-year average major radiation variables (from top to bottom: SWDOWN, GSW, GLW, OLR, and AOD) between CERES observations (left panel) vs. two-way WRF-CMAQ (right panel) in summer, 2008-2012.

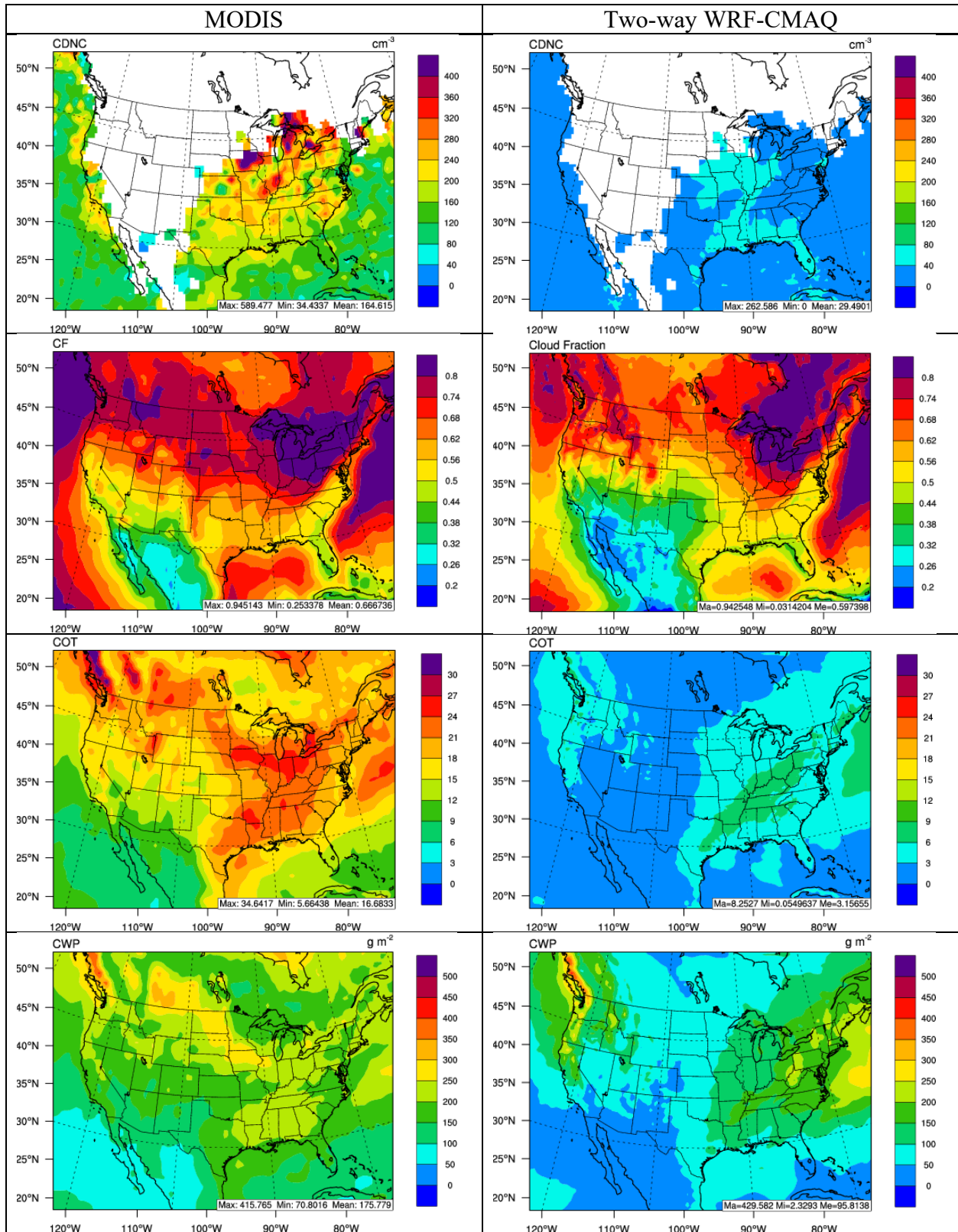


Figure 6. Spatial distribution of 5-year average major cloud variables (from top to bottom: CDNC, CF, COT, and CWP) between MODIS observations (left panel) vs. two-way WRF-CMAQ (right panel) in winter, 2008-2012.

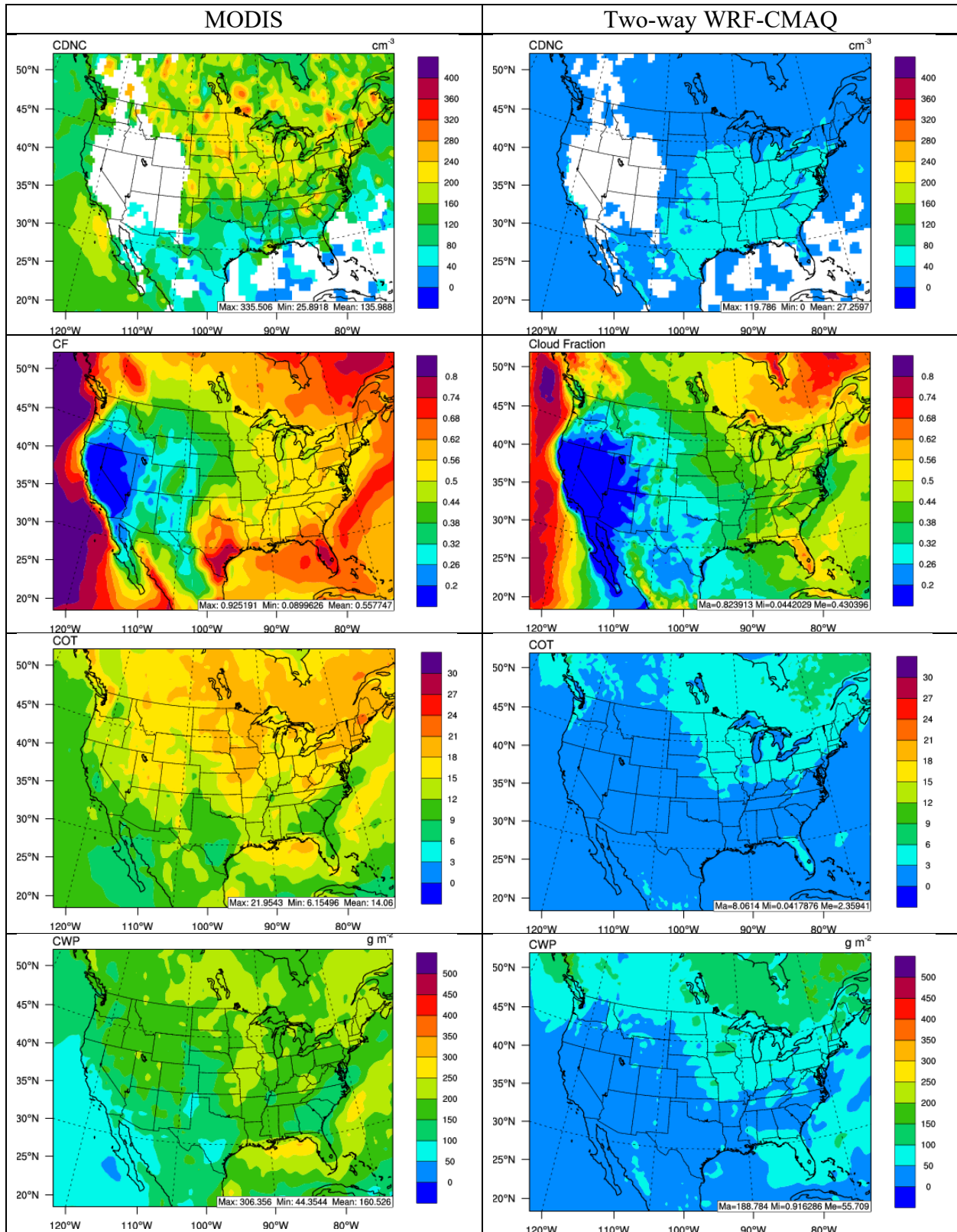


Figure 7. Spatial distribution of 5-year average major cloud variables (from top to bottom: CDNC, CF, COT, and CWP) between MODIS observations (left panel) vs. two-way WRF-CMAQ (right panel) in summer, 2008-2012.

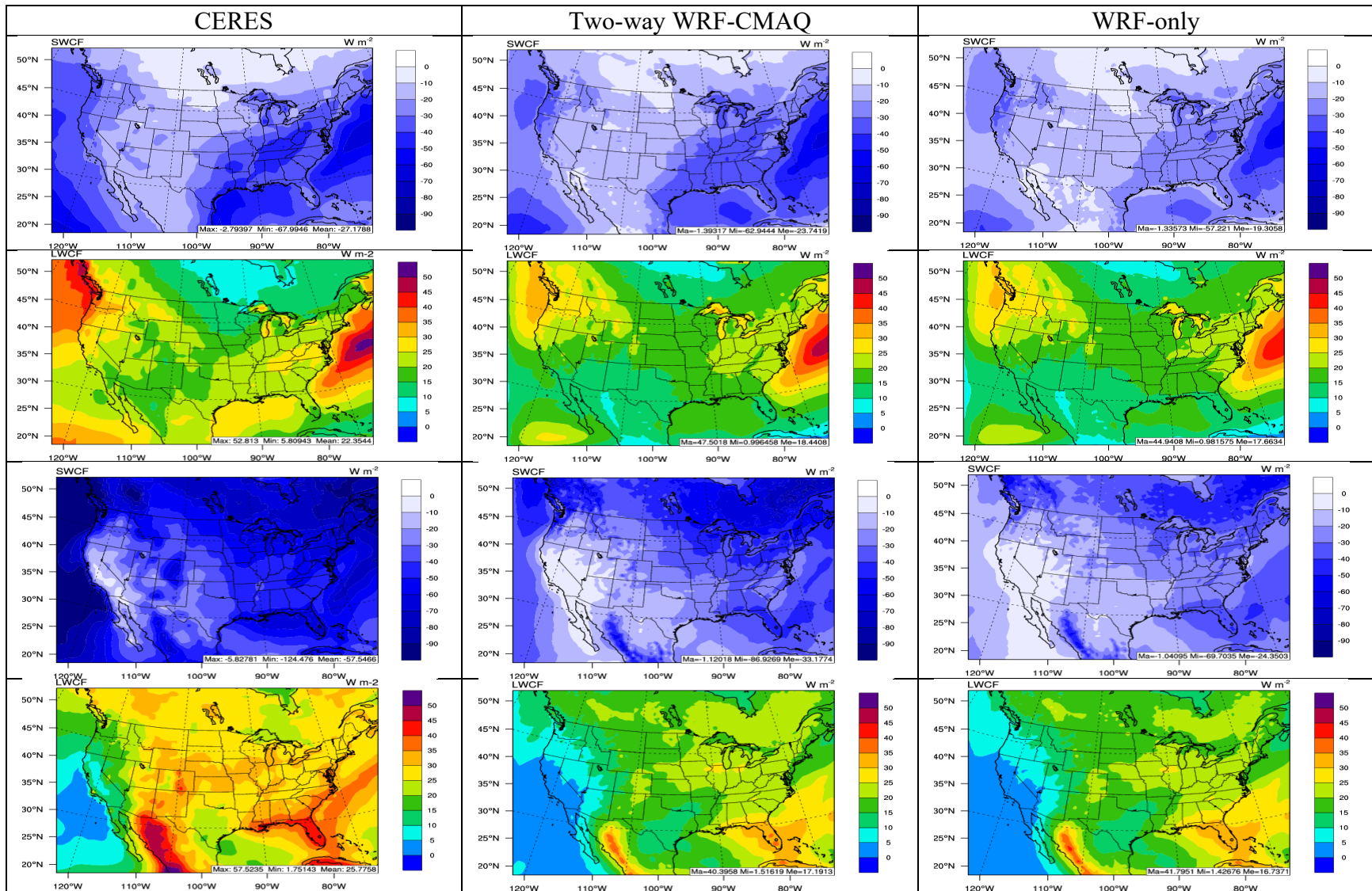


Figure 8. Spatial distribution of 5-year average SWCF in winter, LWCF in winter, SWCF in summer, and LWCF in summer (from top to bottom) between CERES observations (left panel) vs. two-way WRF-CMAQ (center panel) and WRF-only (right panel) in 2008-2012.

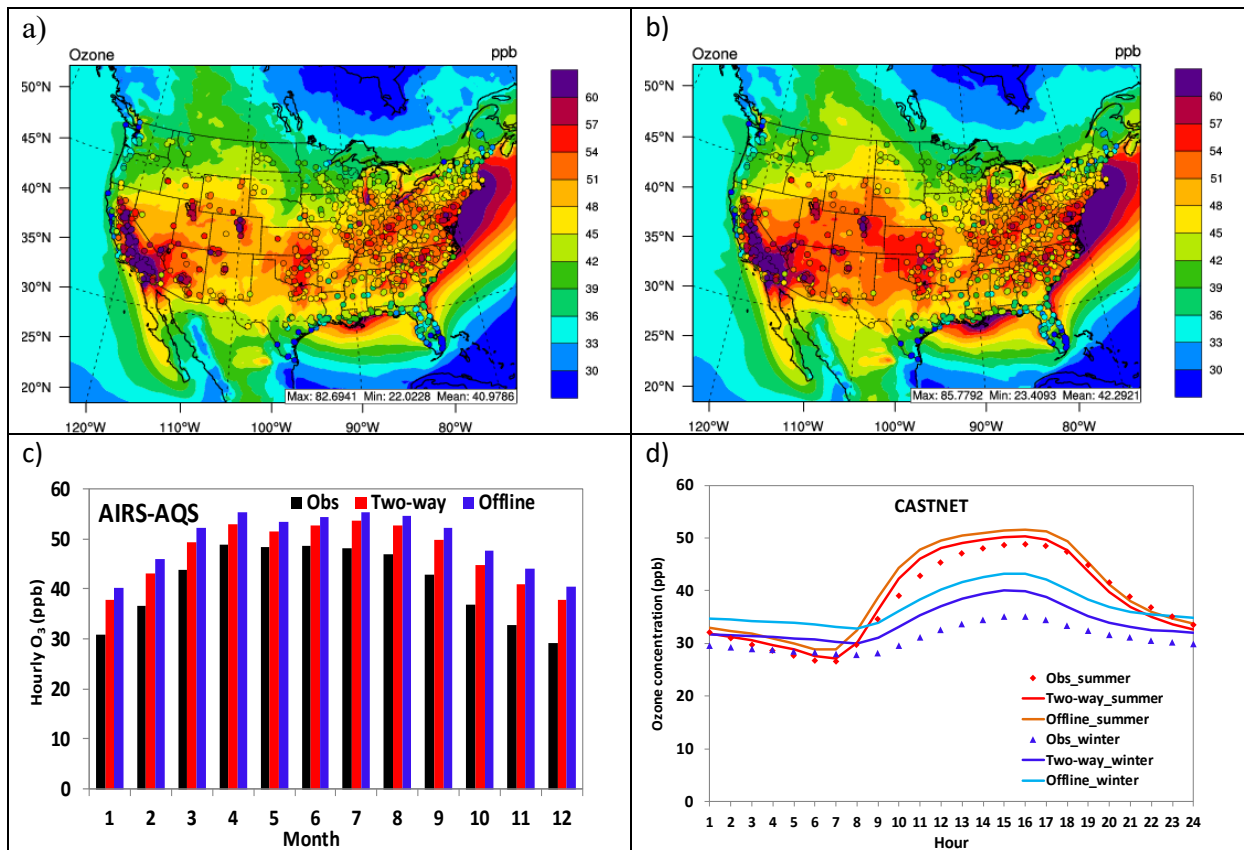


Figure 9. Spatial distributions of 5-year averaged max 8-h O_3 in summer overlaid with observations from AIRS-AQS and CASTNET for a) two-way WRF-CMAQ and b) offline CMAQ; c) bar chart for 5-year average monthly O_3 between observations (black bar), two-way WRF-CMAQ (red bar), and offline CMAQ (blue bar); and d) diurnal plots of observed (dots) vs. simulated (lines) hourly O_3 concentrations against CASTNET for winter (cold colors) and summer (warm colors) in 2008-2012.

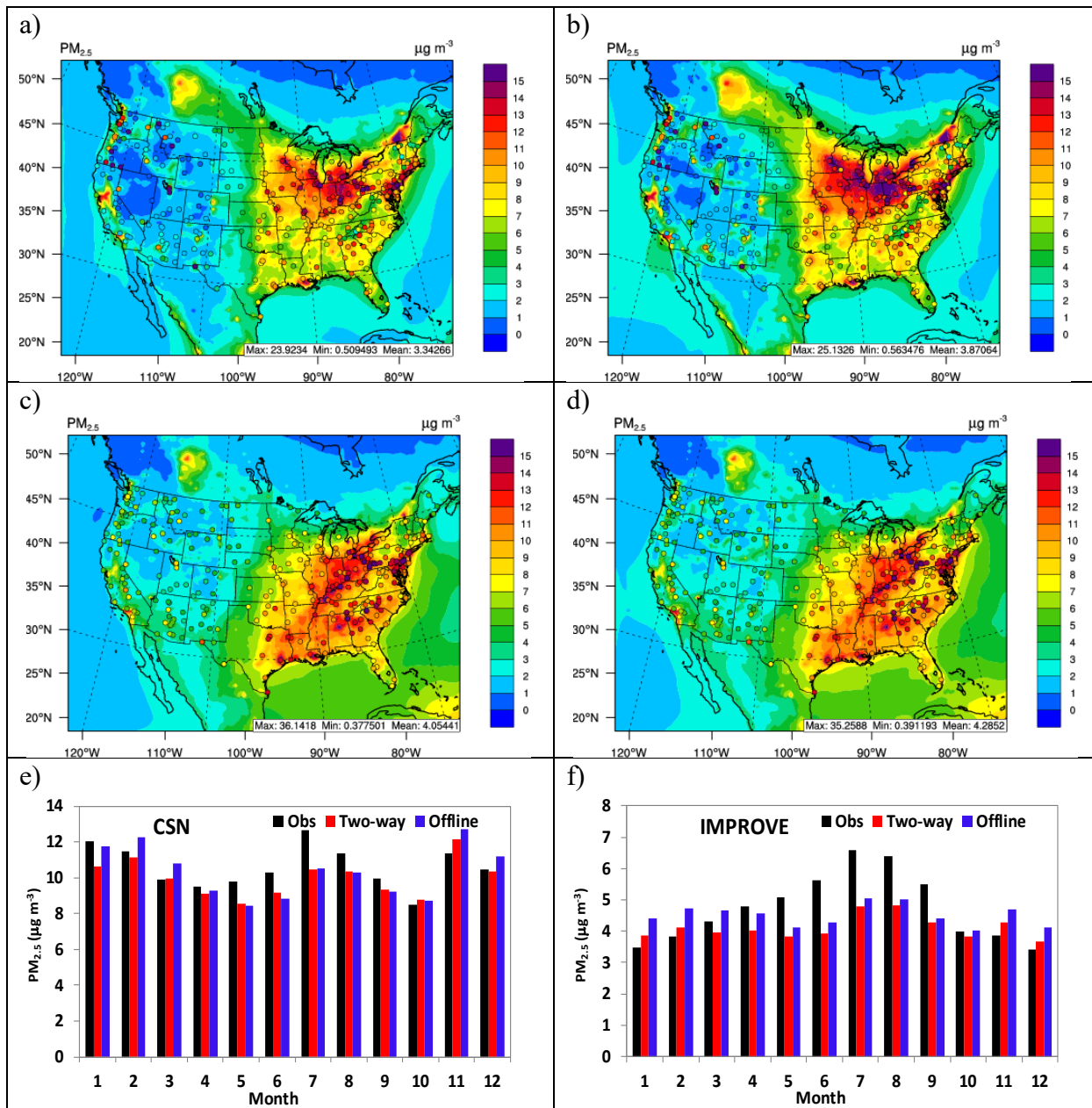


Figure 10. Spatial distributions of 5-year averaged daily PM_{2.5} overlaid with observations from CSN and IMPROVE for two-way WRF-CMAQ in a) winter and c) summer and offline CMAQ in b) winter and d) summer; bar charts for 5-year average monthly PM_{2.5} between observations (black bar), two-way WRF-CMAQ (red bar), and offline CMAQ (blue bar) over e) CSN and f) IMPROVE in 2008-2012.

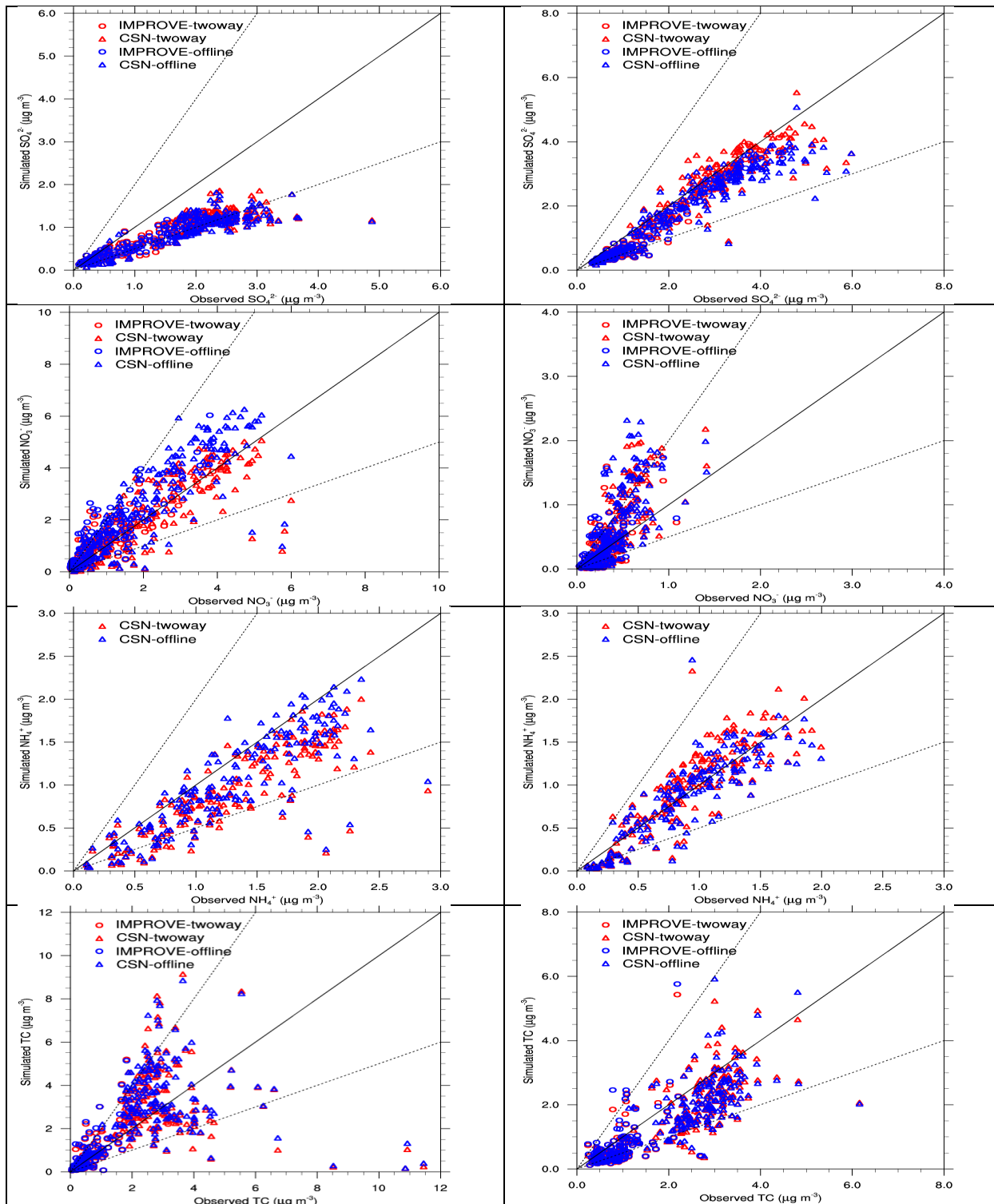


Figure 11. Scatter plots of 5-year averaged PM_{2.5} constituents for SO₄²⁻, NO₃⁻, NH₄⁺, and TC (from top to bottom) between observations and simulations of two-way WRF-CMAQ (red color) and offline CMAQ (blue) in winter (left panel) and summer (right panel), 2008-2012.

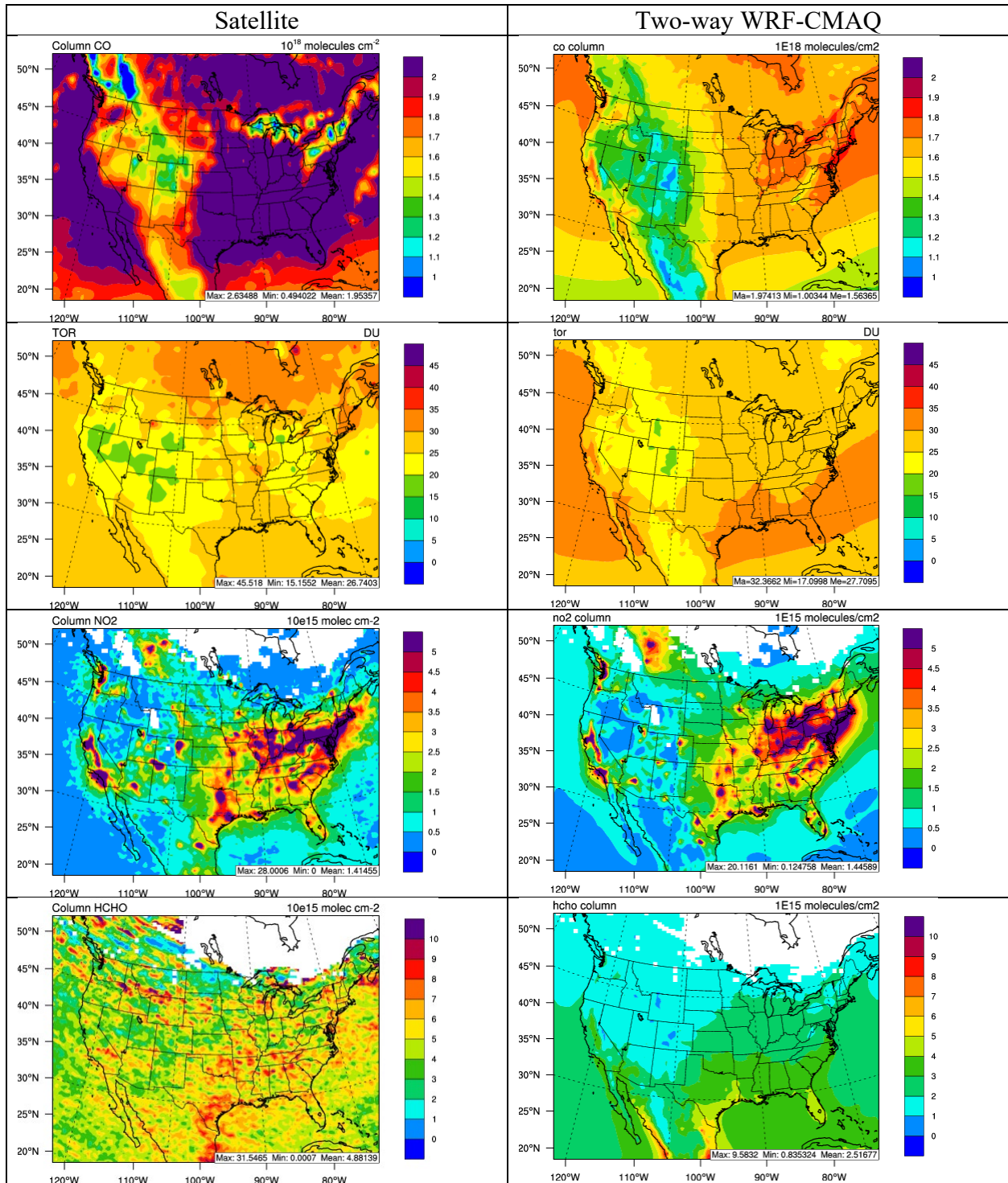


Figure 12. Spatial distribution of 5-year average column abundances (from top to bottom: column CO, TOR, column NO₂, and column HCHO) between various satellite observations (left panel) vs. two-way WRF-CMAQ (right panel) in winter, 2008-2012.

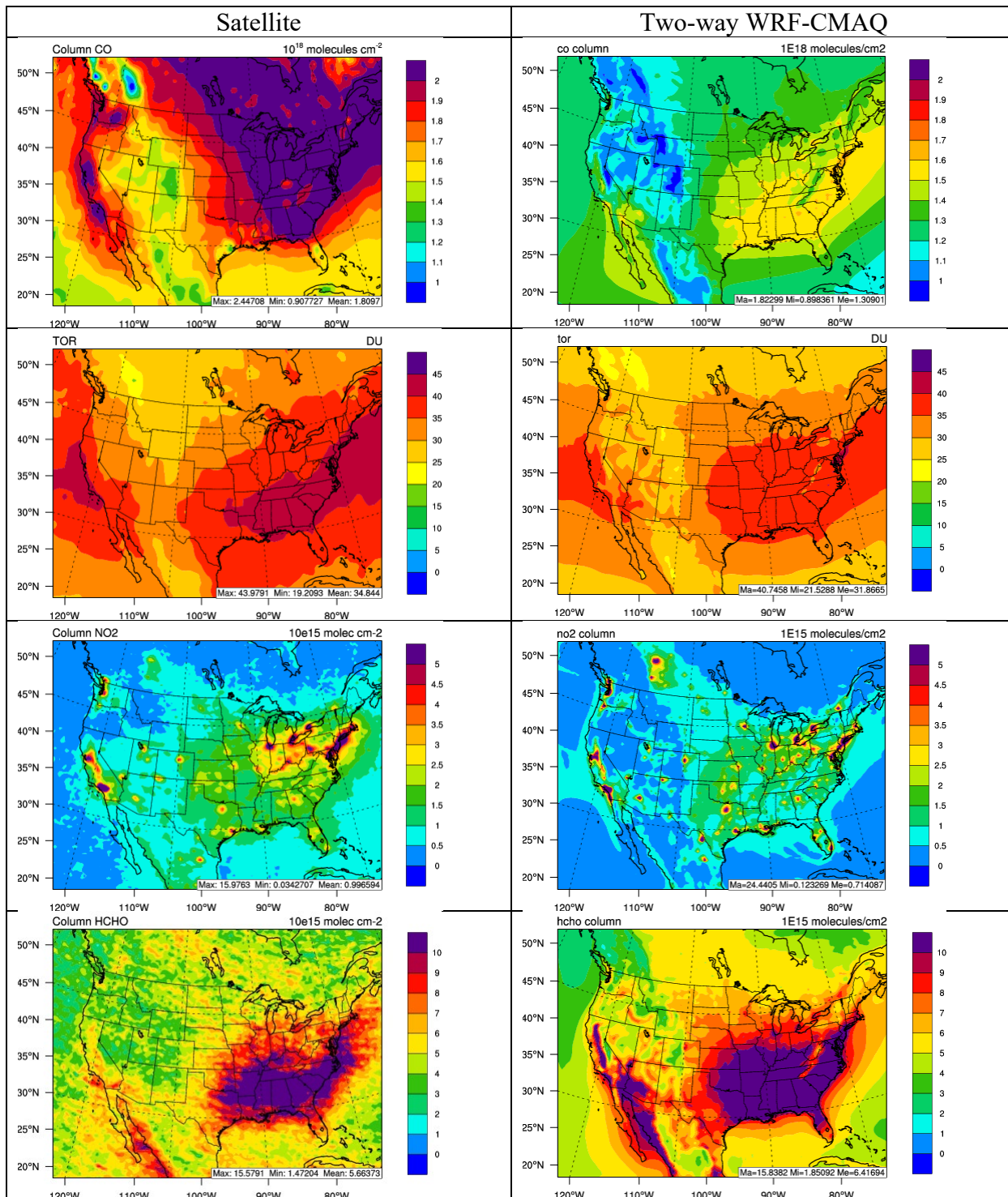


Figure 13. Spatial distribution of 5-year average column abundances (from top to bottom: column CO, TOR, column NO₂, and column HCHO) between various satellite observations (left panel) vs. two-way WRF-CMAQ (right panel) in summer, 2008-2012.

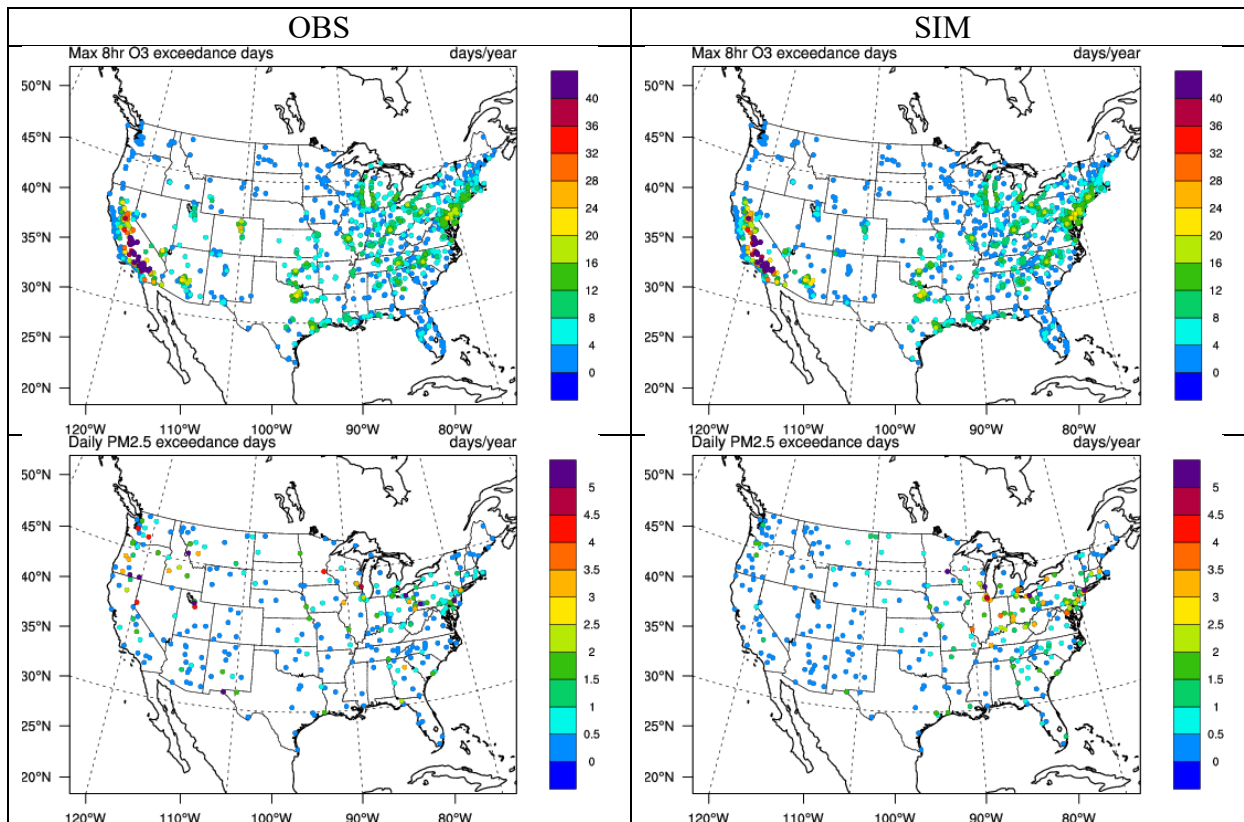


Figure 14. The spatial distribution of 5-year average annual exceedance days of max 8-h O_3 and daily $PM_{2.5}$ between observations (O_3 over the AIRS-AQS/CASTNET network and $PM_{2.5}$ over the IMPROVE/CSN network) and two-way WRF-CMAQ in 2008-2012.

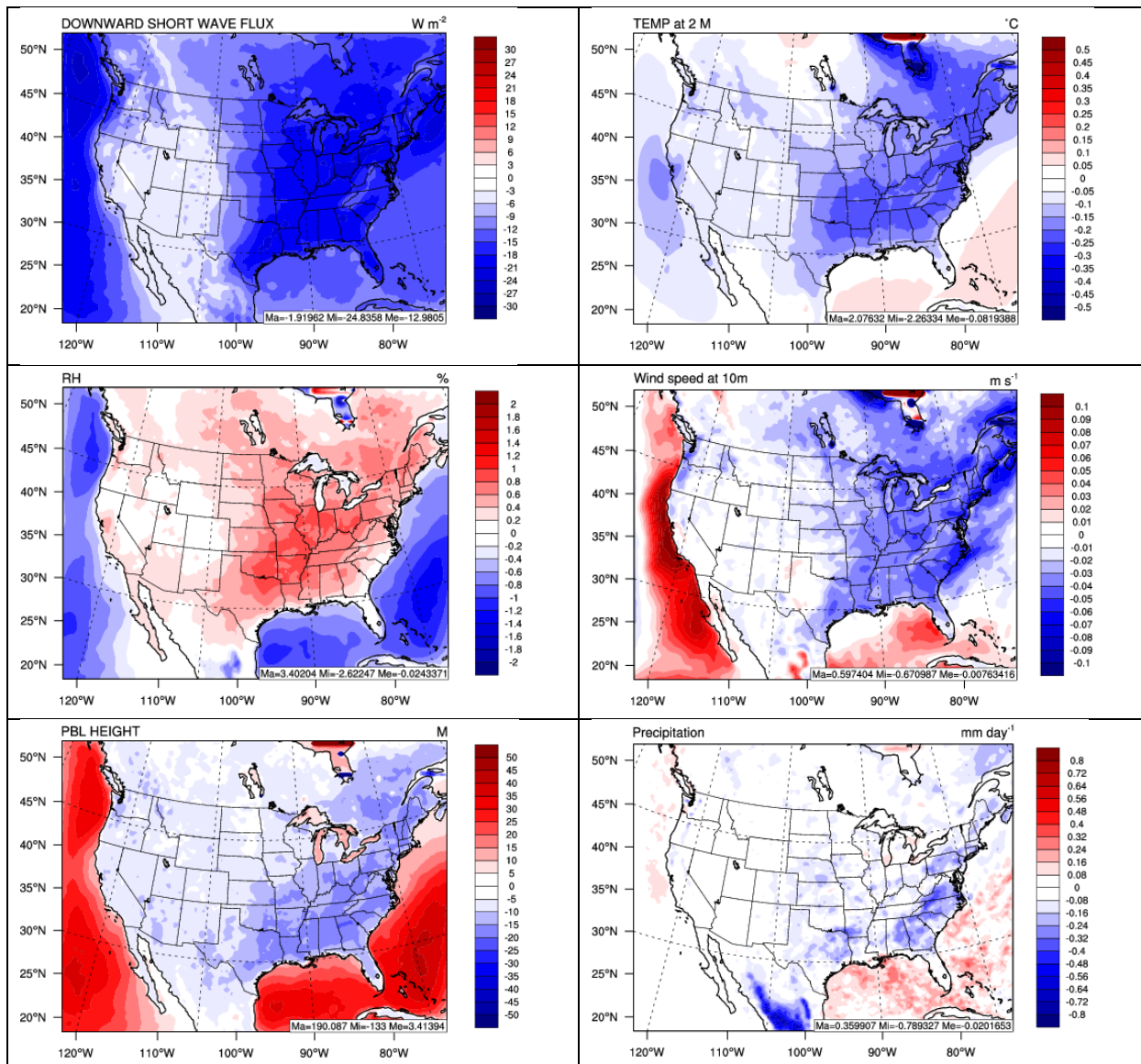


Figure 15. Spatial difference plots (two-way WRF-CMAQ - WRF-only) for major meteorological variables between two-way WRF-CMAQ and WRF-only in 2008-2012.

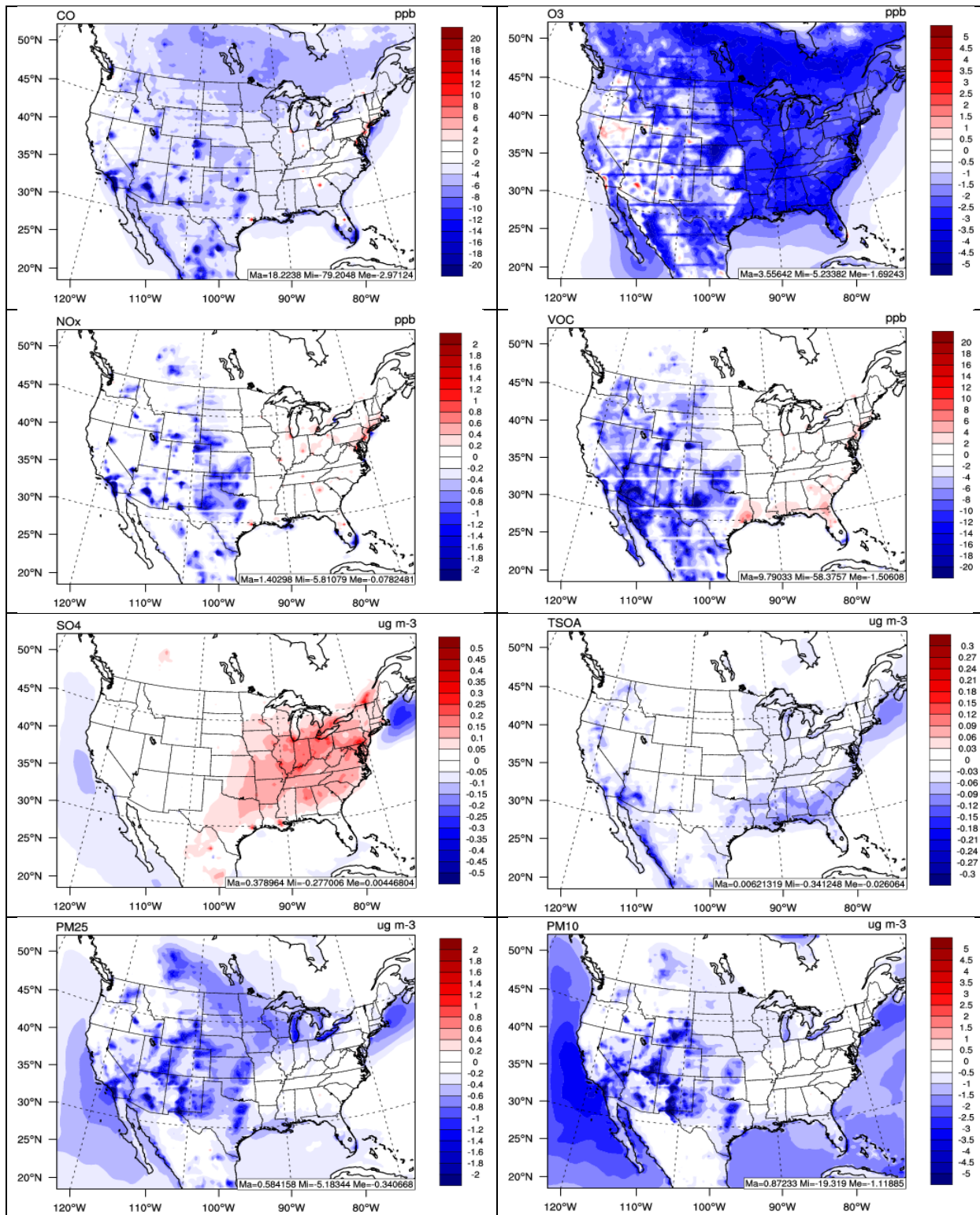


Figure 16. Spatial difference plots (two-way WRF-CMAQ - offline CMAQ) for major chemical species between two-way WRF-CMAQ and offline CMAQ in 2008-2012.